8

MILLIMETER-WAVE POLARIMETRIC RADARS

J. B. Mead and R. E. McIntosh

8.1 Introduction

Radars operating at millimeter wavelengths, at a frequency range between 30 and 300 GHz, have several important advantages over their

microwave counterparts. Millimeter wavelength radars offer greater antenna gain for a given aperture size, better spatial and Doppler resolution, and less susceptibility to clutter and multipath. Waveguide components and antennas scale roughly with wavelength, making the packaging of millimeter-wave systems attractive when miniaturization is important. These advantages come at a price, however. Power output, component sensitivity, and efficiency are harder to achieve at higher frequencies. Also, the greater precision required in manufacturing and the relatively small demand for millimeter-wavelength components forces the cost of a millimeter radar to substantially exceed that of an equivalent microwave system. In addition, atmospheric absorption due to water vapor, oxygen, clouds and rain is greater for millimeter wavelength radars and can be the dominant factor limiting their maximum range.

Recent advances in technology are leading to a better selection of commercially-available components for high performance millimeter-wave systems. Solid-state local oscillator sources are now available throughout the millimeter region and Schottky barrier diode mixers with excellent conversion loss may be combined with solid-state (LO) sources to obtain very efficient receivers. Magnetrons are also available that operate to 100 GHz, while Extended Interaction Oscillators (EIOs) are available that operate up to 270 GHz. High powered amplifiers, such as TWTs and Extended Interaction Amplifiers (EIAs) are also practical up to 95 GHz.

Absorption and scattering by atmospheric liquid water, water vapor and oxygen severely affects the performance of millimeter-wavelength radar systems. In the case of millimeter-wavelength polarimetry, there are three major problems caused by atmospheric effects: (1) attenuation limits the radars range and its effect must be removed if the scattering amplitude of the target is to be accurately determined, (2) backscatter from atmospheric particles can effectively reduce the signal-to-clutter ratio, and (3) some particles, such as raindrops, cause the transmission characteristics of the atmosphere to be anisotropic – thereby distorting the polarization of both the incident and scattered waves.

Figure 8.1 is a plot of atmospheric loss versus range for standard sea level water vapor, temperature and pressure. Attenuation for a rain rate of 10 mm·hr^{-1} is also given. The absorption peaks at 22 and 183 GHz are due to water vapor while the peaks at 60 and 118 are

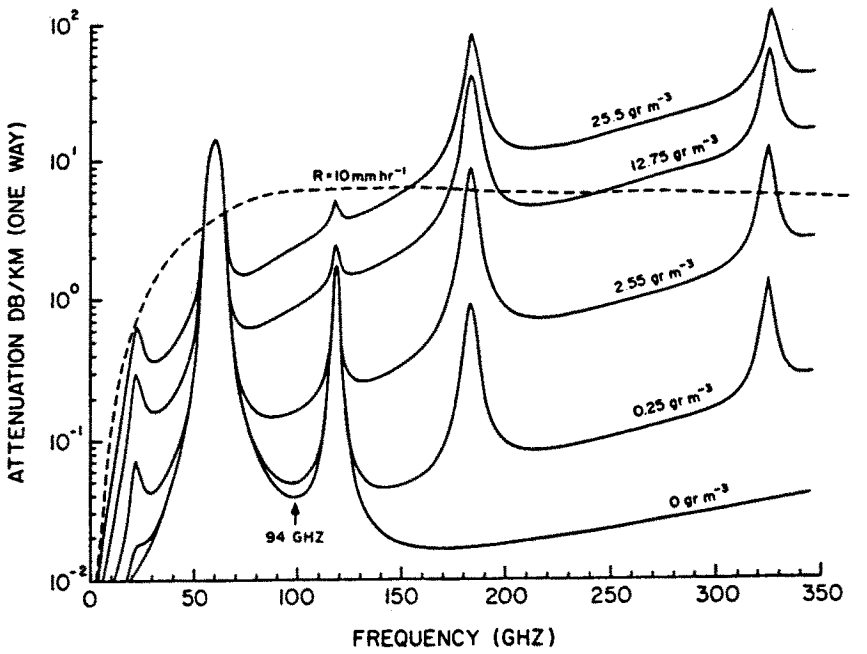

Figure 8.1 Atmospheric gases absorption spectrum at the ground in various humidity conditions indicated by the specific humidity values. Absorption for a 10 mm·h^{-1} rain is also indicated. [Lhermitte, 1988]

due to oxygen. For most millimeter radar applications, the absorption windows at 35, and 95 GHz are used, although radars also operate in the windows at 140 and 220 GHz.

Polarimetric radars, which fully characterize the polarization transformation matrix of a target, can provide significantly more insight into scattering mechanisms than single polarization radars. Recent measurements at microwave frequencies using a polarimetric synthetic aperture radar [Evans, 1988] have proven effective in classifying target homogeneity, scattering mechanisms, and in determining optimal polarizations. Centimeter wavelength polarimetric radars, being sensitive to large scale features of a surface, can discriminate between single bounce surfaces (ocean, sparsely vegetated terrain), double bounce surfaces (ships, urban areas), and diffuse scatterers (tree canopies). In contrast, measurements of foliage using a 225 GHz po-

larimetric radar show a pronounced sensitivity to leaf structure while reflections from the trunk and underlying terrain are highly attenuated.

The dependence of the scattering behavior of a tree canopy at 225 GHz on leaf structure is shown in Figs. 2(a–b). In these figures, the co-polarized polarization signature, defined by Van Zyl [1985] is shown for an Eastern Cottonwood tree having broad leaves (several centimeters across) and for a White Pine tree whose needles are less than .5 mm in diameter. The copolarized signatures are plotted as a function of both the orientation angle, ϕ and the ellipticity angle, τ. The response for the Eastern Cottonwood tree at $\tau = \pm 45°$ is 10 dB below the peak response at $\tau = 0°$, whereas the response for the White Pine tree at $\tau = \pm 45°$ is 6 dB below the peak. These measurements indicate that scattering from the White Pine tree is depolarized more than from a Cottonwood tree. Thus, a millimeter-wave polarimetric radar is able to distinguish the scattering from different types of tree canopies.

Polarimetric measurement methodology

Polarimetric measurement systems operating at millimeter-wavelengths are equivalent to those operating at microwave frequencies. We divide these systems into two categories: (1) those capable of making absolute phase measurements, which are termed coherent, and (2) those capable of relative phase measurements, termed incoherent.

Coherent systems require that the transmitter and receiver share a common reference oscillator like that shown in Fig. 8.3. Two additional requirements are the ability to transmit and receive two nominally orthogonal polarizations. In the system shown in Fig. 8.3, a switch alternates the polarization of the transmitted pulse between two orthogonal polarizations such as vertical and horizontal. An orthomode transducer at the receiver allows the simultaneous detection of both polarizations. Such systems are capable of characterizing the absolute target scattering matrix, **T**, with only two transmitted pulses.

The relative target scattering matrix may be measured incoherently using a system like that shown in Fig. 8.4. In this case, the transmitter must be capable of alternately transmitting two nominally orthogonal polarizations, while the receiver simultaneously samples two orthogonal polarizations and their relative phase. This system assumes that the target and propagation medium are reciprocal, allowing the off-diagonal terms of the scattering matrix to be equated. Relative mo-

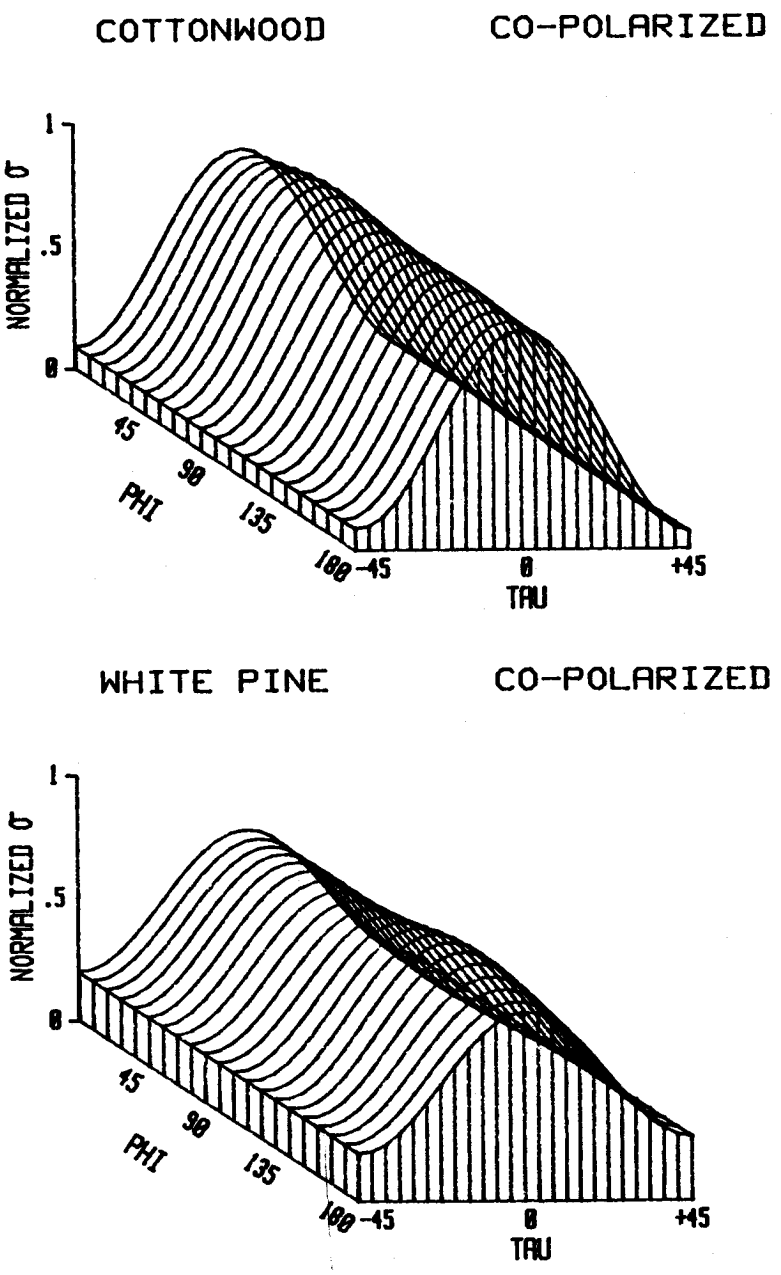

Figure 8.2 (a) Polarization signature for an Eastern Cottonwood tree measured at 225 GHz. (b) Polarization signature for a White Pine tree.

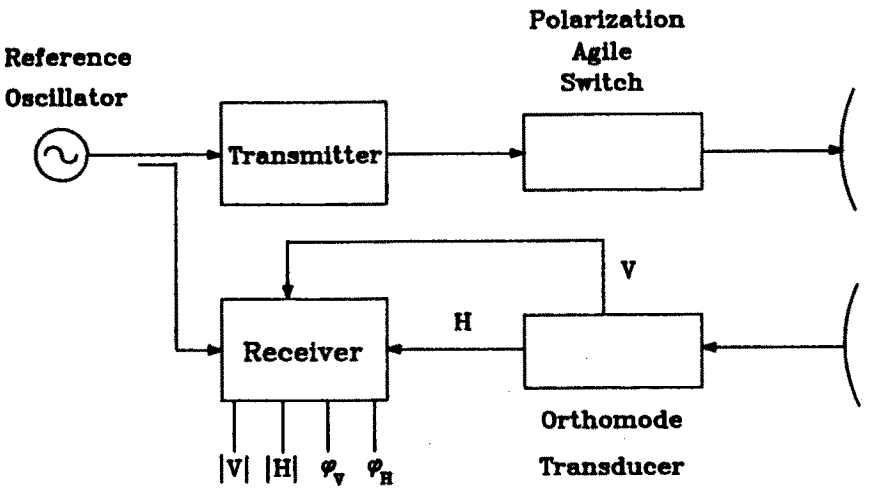

Figure 8.3 Coherent polarimetric radar block diagram for measurement of scattering matrix, T.

tion between the target and the radar system will cause the scattering matrix to vary with time. In order to accurately characterize the instantaneous scattering matrix, it is necessary that the measurements performed by the systems shown in Figs. 3 and 4 be made rapidly to avoid decorrelation of the scene. The average scattering properties of the scene may be found by computing the instantaneous Stokes scattering matrix, M, from T then averaging the elements of M (Huynen, 1970).

In applications where knowledge of the instantaneous scattering matrix is not required, direct measurement of the average Stokes matrix allows the mean scattering properties of a scene to be characterized. Figure 8.5 shows the basic requirements of an incoherent polarimetric radar capable of direct measurement of the Stokes matrix. In this example, the transmitter is capable of producing four different polarizations, i.e., vertical, horizontal, 45° linear, and right-hand circular. The receiver must simultaneously sample two orthogonal polarizations and their relative phase. Such a system can characterize the Stokes

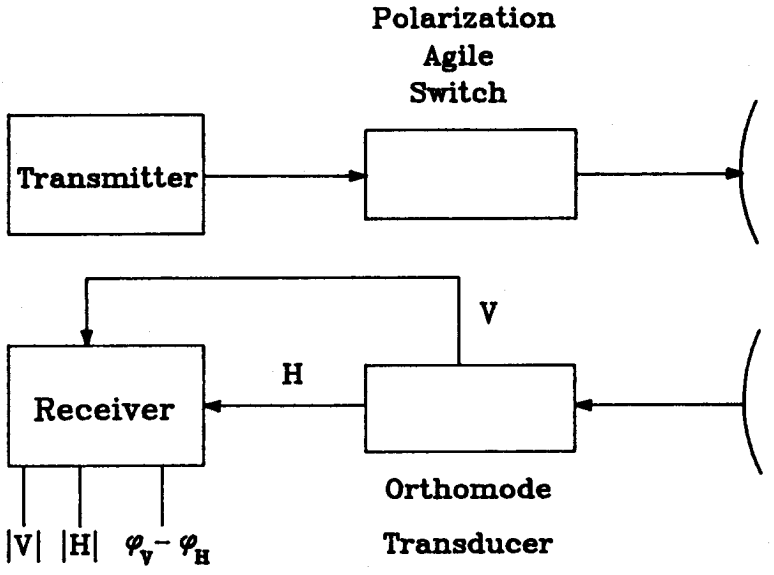

Figure 8.4 Incoherent polarimetric radar block diagram for measurement of scattering matrix, T_r.

scattering matrix by four measurements. Other methods of characterizing target scattering, such as null polarization techniques [Huynen, 1970] and amplitude only techniques [Huynen, 1965] are also possible at millimeter wavelengths.

Details of the various polarimetric measurement schemes described above, as well as hardware requirements, are discussed in section 2 of this chapter. State-of-the-art components are reviewed in section 3, focusing on commercially available transmitter sources, amplifiers, receiver downconverters, Low Noise Amplifiers (LNAs) and waveguide techniques. In section 4, a discussion of measurement errors is presented. This section includes discussion of propagation effects such as attenuation and scattering by atmospheric constituents, anisotropy in rain, and atmospheric turbulence, as well as hardware error sources such as oscillator phase noise, thermal effects, vibration and quantization errors. Two different examples of polarimetric radars are described in section 5: (1) a coherent, polarization-agile 95 GHz radar, and (2) an incoherent 225 GHz polarimeter.

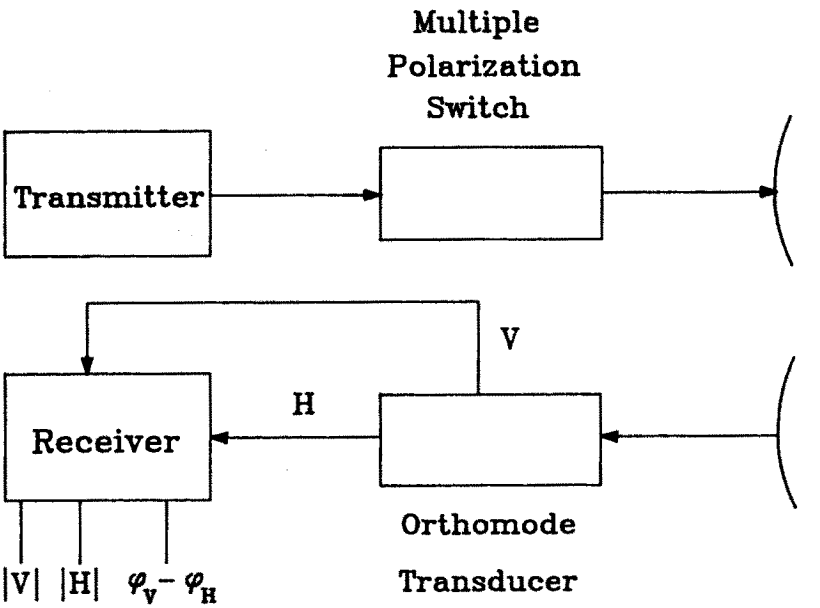

Figure 8.5 Incoherent system for measuring M.

8.2 Polarimetric Measurement Methodologies at Millimeter Wavelengths

Radar scattering from natural and man-made targets is usually described in terms of the target radar cross section, σ, defined as the apparent cross-sectional area of a target assuming isotropic scatter of all power incident upon that target. The power received at the terminals of the radar receive antenna, P_r, is given by the radar range equation

$$P_r = \frac{P_t G_t G_r \lambda^2 \sigma}{(4\pi)^3 R^4} \tag{2.1}$$

where P_t is transmitted power, G_t and G_r are the transmit and receive antenna gains, λ is the radar wavelength, and R the target range. Equation (2.1) may be used to estimate system performance in the presence of noise or to compute σ from measured power. In the case of polarimetric radars, σ refers to the radar cross section for specific

transmit and receive polarizations. Equation (2.1) may be modified for surface targets using the normalized radar cross section, σ°, which is the radar cross section per unit area of the surface. For surface targets $\sigma = (\sigma^\circ A_i)$ where A_i is the footprint area illuminated by the radar antennas.

The polarization state of a TEM wave traveling in the $+z$ direction can be described in terms of the ellipse traced out by the electric field vector at the point $z = z_0$, as shown in Fig. 8.6. The ellipse parameters, ϕ and τ, completely specify the polarization state of the wave and are expressed in terms of electric field quantities by

$$\tau = \frac{1}{2}\sin^{-1}\left(\frac{2|V|\,|H|\sin\delta}{|V|^2 + |H|^2}\right) \tag{2.2}$$

$$\phi = \frac{1}{2}\tan^{-1}\left(\frac{2|V|\,|H|\cos\delta}{|V|^2 - |H|^2}\right) \tag{2.3}$$

where $|V|$ and $|H|$ represent the magnitude of the electric field in the vertical and horizontal planes, and δ is the phase difference between the vertical and horizontal field components. Right-hand waves are represented by $\tau > 0$. A receiver capable of measuring $|V|$, $|H|$ and δ is therefore able to measure the instantaneous polarization state of an incoming wave.

The scattering transformation of a single target is completely characterized by the complex target scattering matrix, $\mathbf{T}$, i.e.

$$\mathbf{E}_s = \mathbf{T}\mathbf{E}_t \tag{2.4}$$

where the column matrix $\mathbf{E}_t$ represents the field incident on the target and the column matrix $\mathbf{E}_s$ represents the scattered field at the observation point a distance R from the target. Selecting vertical and horizontal polarization as a convenient orthogonal basis, $\mathbf{E}_s$ and $\mathbf{E}_t$ are given by

$$\mathbf{E}_i = \begin{bmatrix} |H|e^{i\alpha_H} \\ \\ |V|e^{i\alpha_V} \end{bmatrix} \tag{2.5}$$

where α_H and α_V are the absolute phase of the horizontal and vertical field components and $\mathbf{T}$ is given by

$$\mathbf{T} = \frac{e^{-ikR}}{R}\begin{bmatrix} t_{HH} & t_{HV} \\ t_{VH} & t_{VV} \end{bmatrix} \tag{2.6}$$

Where $t_{mn} = \sqrt{4\pi\sigma_{m,n}}e^{-i\psi_{m,n}}$, $\sqrt{4\pi\sigma_{m,n}}$ is the magnitude of the scattering coefficient, $\psi_{m,n}$ is relative phase, and m, n indicate the receive and transmit polarizations, respectively. Reciprocity requires that $t_{HV} = t_{VH}$ for monostatic measurements (transmitter and receiver co-located) so **T** is completely characterized by six real values.

a. Coherent Measurements of the Scattering Matrix

Although various systems can be devised for measuring the scattering matrix, **T**, these systems are subject to the following constraints:

1. The radar must be phase coherent, i.e., the received phase must be measured relative to the phase of the transmit signal, and
2. In the case of fluctuating targets, the measurement of all matrix elements must be made more rapidly than the target decorrelation time.

The second constraint usually requires a polarization-agile system, capable of transmitting two orthogonal polarizations in rapid succession. Such a system is shown schematically in Fig. 8.3. A common phase-locked oscillator (PLO) is used for both transmitter and receiver which provides a means of storing the transmitted phase for comparison with the scattered voltage. Orthogonal receive channels (often V and H) are employed allowing simultaneous measurement of t_{Vx} and t_{Hx} where $x = H$ or V. In the case of a pulsed radar system, the complete scattering matrix may be measured by two pulses. The polarization agile assembly must therefore be able to switch at the radar's pulse repetition frequency (PRF), typically on the order of several KHz. This type of polarimetric radar is more versatile than the other systems discussed in this chapter because it can rapidly measure the complete target scattering matrix as well as measure Doppler information for each element of the matrix.

b. Incoherent Measurement of the Scattering Matrix

The absolute phase of **T** is not always required, so the relative scattering matrix, $\mathbf{T}_r$, is often measured. $\mathbf{T}_r$ is completely characterized by only five real numbers. A radar capable of measuring $\mathbf{T}_r$ directly is subject to the following constraints:

1. The relative phase between orthogonal receive channels must be measured, and
2. Measurements of rapidly fluctuating targets must be made more rapidly than the target decorrelation time.

As in the coherent case, the second constraint requires a polarization agile transmitter as shown in Fig. 8.4. Measurements of the relative scattering matrix elements t_V and t_H are made simultaneously. Using reciprocity, the off-diagonal elements of the matrix are equated to yield the final result. Equating the off-diagonal elements is valid so long as the target has not changed appreciably during the interpulse period.

c. *Incoherent Measurement of Stokes Scattering Matrix*

A more general description of wave polarization, which may account for partially polarized waves, is given by the Stokes vector $\mathbf{g}$ [Huynen, 1970]

$$\mathbf{g} = \begin{bmatrix} g_0 \\ g_1 \\ g_2 \\ g_3 \end{bmatrix} \tag{2.7}$$

where $g_0 = |H|^2 + |V|^2, g_1 = |H|^2 - |V|^2, g_2 = 2|V|\ |H| \cos\delta$ and $g_3 = 2|V|\ |H| \sin\delta$. Furthermore, the scattering behavior of an arbitrary point or distributed target may be characterized in terms of the average Stokes scattering matrix $\mathbf{M}$. The power received by an antenna whose polarization state is specified by the Stokes vector $\mathbf{g}_{rc}$, can be obtained in terms of the Stokes matrix, $\mathbf{M}$, of the target and the Stokes vector of the transmit antenna polarization, $\mathbf{g}_{tr}$ as follows:

$$P_{rec} = k\mathbf{g}_{rc}^T \mathbf{M} \mathbf{g}_{tr} \tag{2.8}$$

where k accounts for propagation effects between the radar and the target, and $\mathbf{g}^T$ is the transpose of $\mathbf{g}$.

The average Stokes matrix of the target may be measured by sequentially illuminating the target with vertical ($\phi = 90°, \tau = 0°$), horizontal ($\phi = 0°, \tau = 0°$), 45 degree linear ($\phi = 45°, \tau = 0°$), and right hand circular (ϕ arbitrary, $\tau = 45°$) polarized waves. The ideal Stokes vectors for these waves are

$$\mathbf{g}_v = \begin{bmatrix} 1 \\ -1 \\ 0 \\ 0 \end{bmatrix}, \quad \mathbf{g}_h = \begin{bmatrix} 1 \\ 1 \\ 0 \\ 0 \end{bmatrix}, \quad \mathbf{g}_{45} = \begin{bmatrix} 1 \\ 0 \\ 1 \\ 0 \end{bmatrix} \quad \text{and} \quad \mathbf{g}_{RC} = \begin{bmatrix} 1 \\ 0 \\ 0 \\ 1 \end{bmatrix} \tag{2.9}$$

respectively. The waves that are scattered by a target when vertical, horizontal, 45 degree linear and right hand circular polarized waves are

transmitted can also be expressed as Stokes vectors as follows:

$$\mathbf{r}_v = \begin{bmatrix} r_{0v} \\ r_{1v} \\ r_{2v} \\ r_{3v} \end{bmatrix}, \quad \mathbf{r}_h = \begin{bmatrix} r_{0h} \\ r_{1h} \\ r_{2h} \\ r_{3h} \end{bmatrix}, \quad \mathbf{r}_{45} = \begin{bmatrix} r_{0_{45}} \\ r_{1_{45}} \\ r_{2_{45}} \\ r_{3_{45}} \end{bmatrix} \quad \text{and} \quad \mathbf{r}_{RC} = \begin{bmatrix} r_{0_{RC}} \\ r_{1_{RC}} \\ r_{2_{RC}} \\ r_{3_{RC}} \end{bmatrix} \tag{2.10}$$

Each of the Stokes parameters that comprise the above Stokes vectors may be determined by a receiver capable of measuring $|V|$, $|H|$ and δ. Furthermore, the parameters can be used to determine the Stokes matrix of the target by the expression:

$$\begin{bmatrix} M_{01} & M_{02} & M_{03} & M_{04} \\ M_{11} & M_{12} & M_{13} & M_{14} \\ M_{21} & M_{22} & M_{23} & M_{24} \\ M_{31} & M_{32} & M_{33} & M_{34} \end{bmatrix}$$

$$= \frac{1}{2} \begin{bmatrix} (r_{0v} + r_{0h}) & (r_{0h} - r_{0v}) & (2r_{0_{45}} - r_{0v} - r_{0h}) & (2r_{0_{RC}} - r_{0v} - r_{0h}) \\ (r_{1v} + r_{1h}) & (r_{1h} - r_{1v}) & (2r_{1_{45}} - r_{1v} - r_{1h}) & (2r_{1_{RC}} - r_{1v} - r_{1h}) \\ (r_{2v} + r_{2h}) & (r_{2h} - r_{2v}) & (2r_{2_{45}} - r_{2v} - r_{2h}) & (2r_{2_{RC}} - r_{2v} - r_{2h}) \\ (r_{3v} + r_{3h}) & (r_{3h} - r_{3v}) & (2r_{3_{45}} - r_{3v} - r_{3h}) & (2r_{3_{RC}} - r_{3v} - r_{3h}) \end{bmatrix} \tag{2.11}$$

In practice, the actual transmit Stokes parameters are determined as part of the system calibration. This leads to more complicated expressions for M than given by (2.10). In general, M is given by

$$\mathbf{M} = \begin{bmatrix} 1 & 0 & 0 & 0 \\ 0 & 1 & 0 & 0 \\ 0 & 0 & 1 & 0 \\ 0 & 0 & 0 & -1 \end{bmatrix} \mathbf{R}_{sc} \mathbf{G}_{tr}^{-1} \tag{2.12}$$

where $\mathbf{R}_{sc}$ and $\mathbf{G}_{tr}$ are given by

$$\mathbf{R}_{sc} = \begin{bmatrix} r_{0V} & r_{0H} & r_{045} & r_{0RC} \\ r_{1V} & r_{1H} & r_{145} & r_{1RC} \\ r_{2V} & r_{2H} & r_{245} & r_{2RC} \\ r_{3V} & r_{3H} & r_{345} & r_{3RC} \end{bmatrix} \quad \text{and} \tag{2.13}$$

$$\mathbf{G}_{tr} = \begin{bmatrix} g_{0V} & g_{0H} & g_{045} & g_{0RC} \\ g_{1V} & g_{1H} & g_{145} & g_{1RC} \\ g_{2V} & g_{2H} & g_{245} & g_{2RC} \\ g_{3V} & g_{3H} & g_{345} & g_{3RC} \end{bmatrix} \tag{2.14}$$

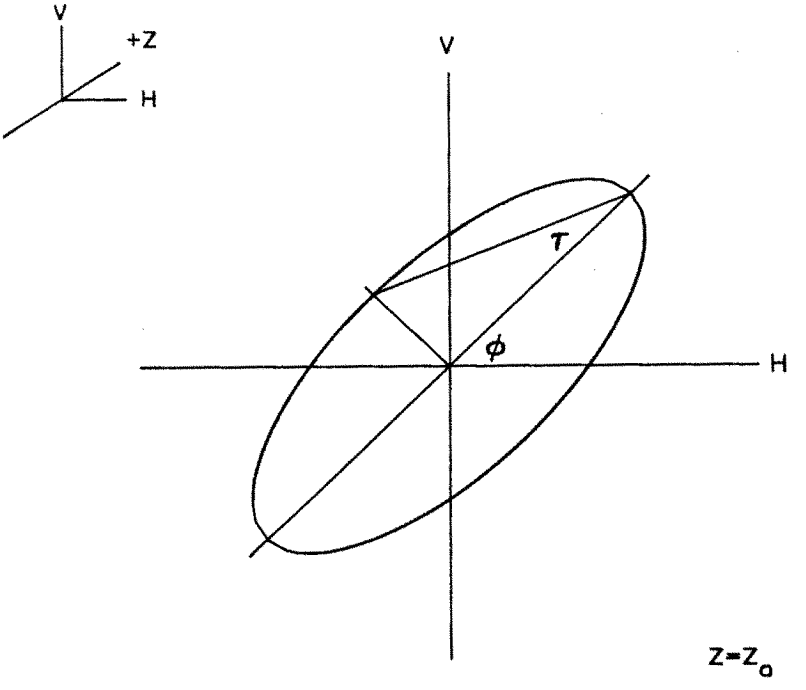

Figure 8.6 Ellipse parameters ϕ (orientation) and τ (ellipticity).

A radar capable of making direct measurements of the Stokes scattering matrix elements is shown in Fig. 8.4. The measurements described above may be accomplished at millimeter wavelengths by mechanically switching the transmitter between the various polarization states. In such cases, it takes longer to characterize the scattering properties of a target than with the other described methods.

d. Hardware Requirements for Polarimetric Radars

Hardware requirements for a polarimetric radar are based not only on the measurement methodology chosen, but on the requirements of the measurement program. System requirements for an airborne imaging polarimeter, for instance, are likely to be different than for a laboratory polarimeter making measurements of point targets. Various methods of configuring both transmitter and receiver are discussed below.

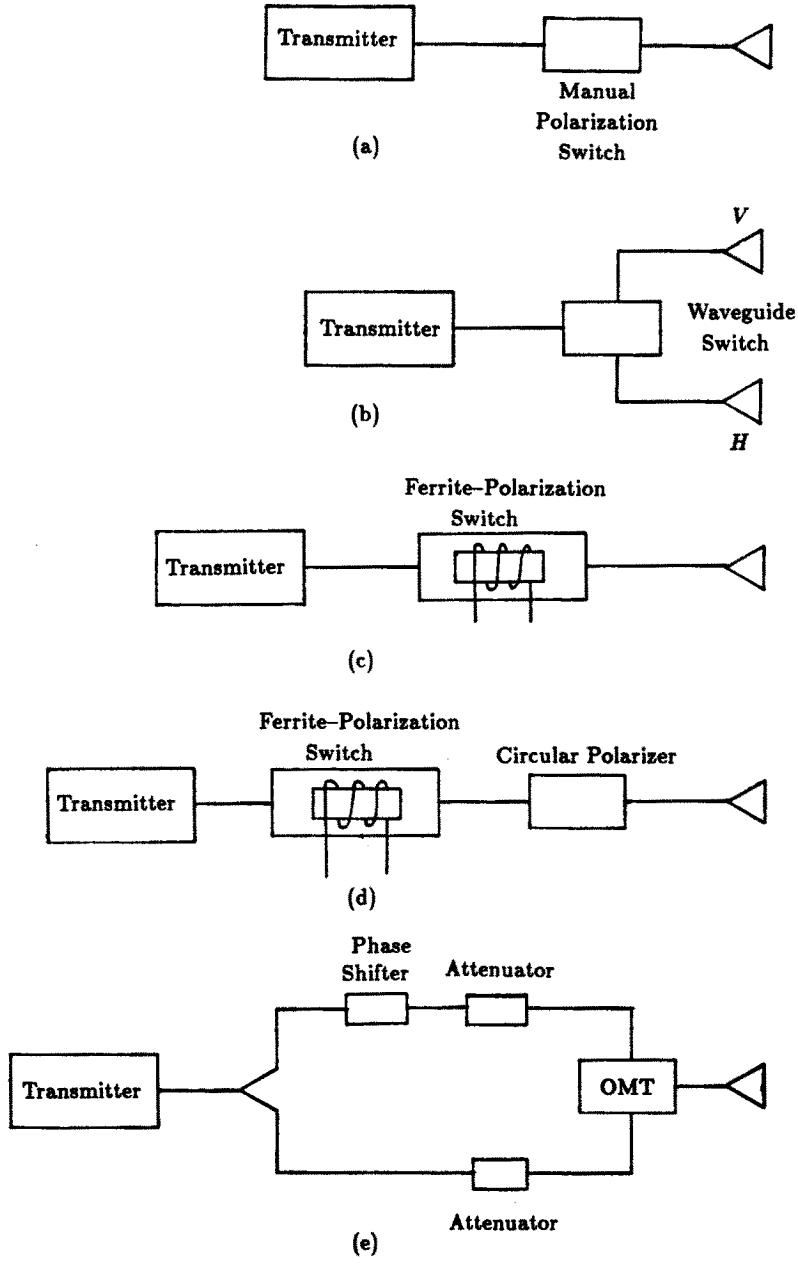

Figure 8.7 (a–e) Various polarization agile systems.

The transmitter must be capable of either transmitting two nominally orthogonal polarizations for direct measurements of the scattering matrix, or be able to transmit several linearly independent polarizations for incoherent measurements of the Stokes matrix. For systems like that illustrated in Fig. 8.5, a simple manual switch like that shown in Fig. 8.7(a) is adequate. For systems requiring rapid measurements of scattering parameters, a system capable of rapidly switching between orthogonal polarizations is necessary. One way to achieve this is shown in Fig. 8.7(b) where a switch is employed after the final amplifier to switch between orthogonal antennas. A disadvantage of such an approach is the additional cost of using two separate transmit antennas. Another effective option, shown in Fig. 8.7(c), employs a ferrite polarization switch, capable of generating any linear polarization state. Addition of a circular-polarizer after the polarization switch, Fig. 8.7d, permits transmission of the various elliptical polarizations lying along the great circle of the Poincaré sphere passing through RHC, H, LHC and V polarizations. Ferrite waveguide switches and circular polarizers are now available for W-band and below (below 110 GHz). General polarization agility can be achieved using the system shown in Fig. 8.7e.

A polarimetric radar receiver must sample two nominally orthogonal polarizations in order to completely characterize the instantaneous scattered wave. One solution to this problem is to employ a dual channel receiver that simultaneously samples the voltage from separate, orthogonally polarized antennas as shown in Fig. 8.8a. Alternately, a single dual-polarized antenna may be employed, as shown in Fig. 8.8b. These receivers can completely characterize the backscattered wave in one pulse. A third option, employing a single receiver channel switched between the two outputs of a dual polarized antenna is shown in Fig. 8.8c. This method requires two samples of the received signal to characterize the backscattered wave. The polarization splitter shown schematically in Fig. 8.8b can be implemented by use of a waveguide orthomode transducer (OMT), for frequencies below 110 GHz, or by use of a polarization-splitting wire grid as shown in Fig. 8.9 at higher frequencies. If the orthogonal receiver channels are left and right-hand circularly polarized, a circular-to-linear polarizer may be inserted before the OMT or wire grid.

When only a single antenna is desired, a circulator may be inserted in the transmit path as shown in Fig. 8.10. Practical low-loss waveguide circulators are currently available for frequencies to W-band. Quasi-

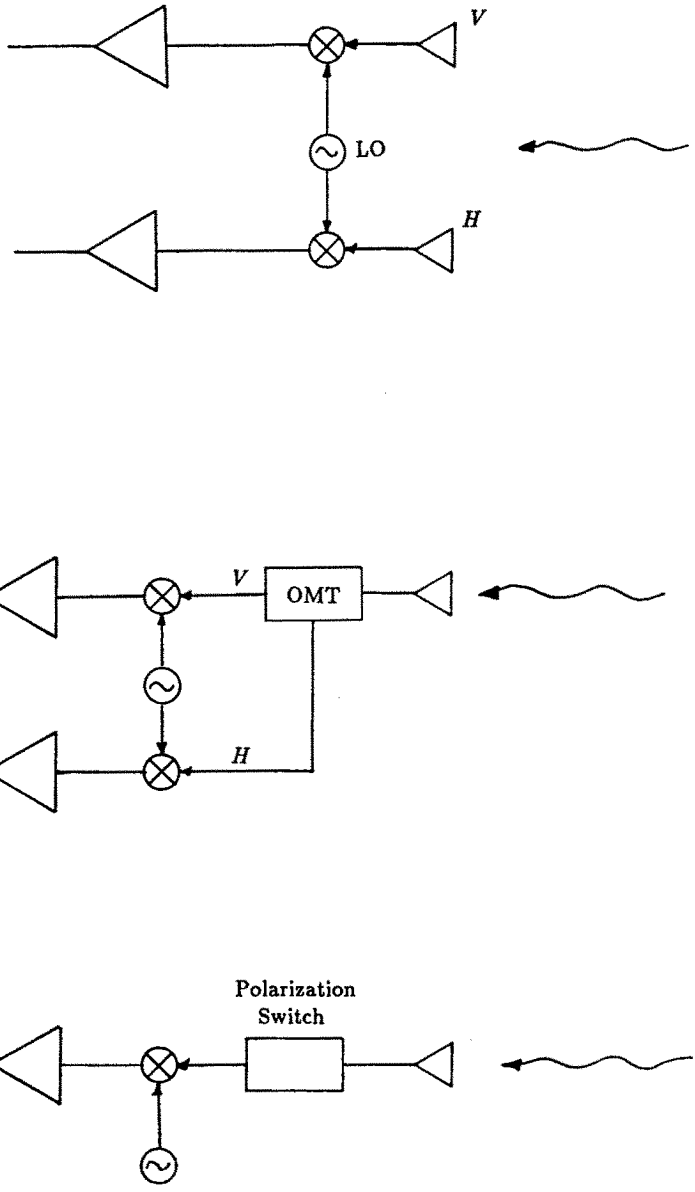

Figure 8.8 (a–c) Various dual polarization receiver configurations.

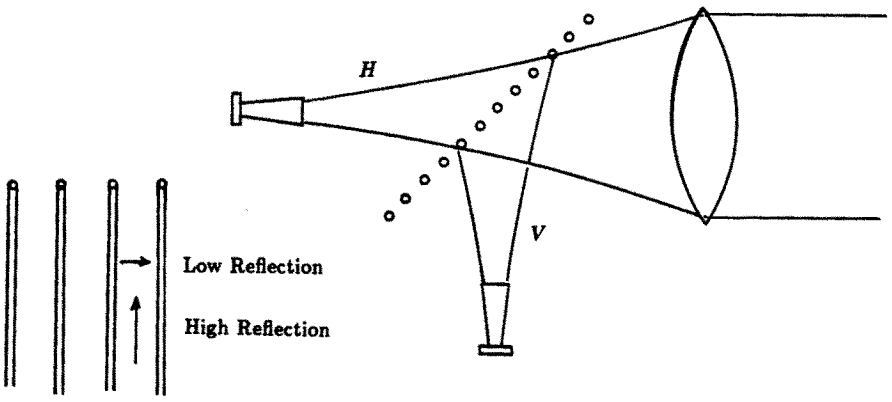

Figure 8.9 Wire grid polarization duplexer.

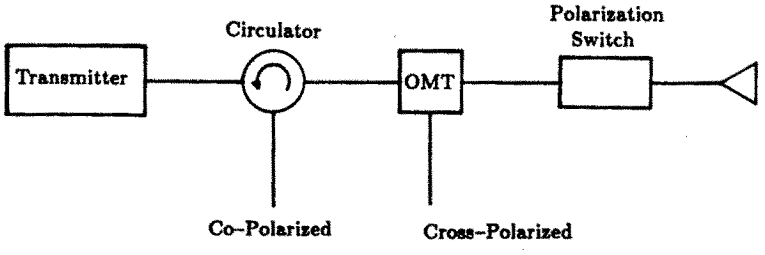

Figure 8.10 Single antenna system.

optical implementation of a circulator has also been demonstrated at 150 GHz with 30 percent bandwidth, 20 dB isolation and 0.2 dB insertion loss (Millitech, 1986).

Good antenna polarization characteristics are essential for polarimetric measurements, especially when software vector correction techniques cannot be used. For example, meteorological radars that measure the circular depolarization ratio

$$CDR = 10\log(\langle RL\rangle/\langle RR\rangle) \tag{2.15}$$

must measure the power from the RHC and LHC receive antennas ($\langle RR\rangle$ and $\langle RL\rangle$, respectively) when the transmit polarization is RHC. Data rates for a scanning meteorological radar can be very high, and thus signal processing must be kept to a minimum due to signal processing speed limitations. This may prevent the measured data from being corrected using the techniques described in section 5. In order to measure CDR values down to −30 dB, integrated antenna cross-pol must be held below −36 dB. This requires careful antenna design and testing.

8.3 Millimeter-Wave Components

a. Introduction

Components for millimeter-wavelength polarimetric radars are often scaled versions of devices used at RF and microwave frequencies. Familiar RF devices such as coaxial cables and field effect transistors are practical for frequencies up to approximately 40 GHz. However, waveguides, klystrons, Gunn diodes and other components are used throughout the millimeter region. A common problem that these devices have at millimeter wavelengths is that they require delicate resonant and waveguiding structures to handle high current and power densities. For example, resistive loss in waveguide may reach several tenths of a dB per inch above 100 GHz. Quasi-optical waveguide, which allows for free-space propagation of energy with periodic refocusing elements, has loss as low as .05 dB per inch at 250 GHz, and therefore is preferable in many applications. A discussion of commonly used millimeter-wave devices is presented below.

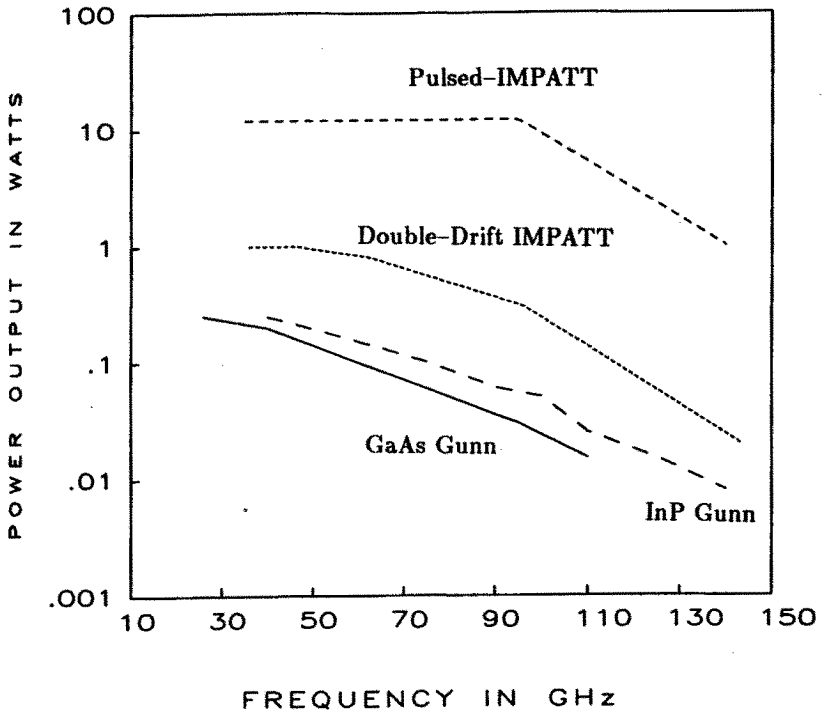

Figure 8.11 Power output for CW and pulsed Gunn and IMPATT diodes.

b. Solid-State Gunn and IMPATT Devices

Two solid-state devices that have widespread application as sources of millimeter-wave power are the Gunn and Impact Avalanche Transit-Time (IMPATT) diodes. Gunn diodes are typically manufactured using Gallium Arsenide (GaAs) or Indium Phosphide (InP), with the InP devices providing higher efficiency, power output and lower AM noise. Because Gunn oscillators have superior AM/FM noise characteristics as compared with IMPATT devices, they are usually preferred as LO sources. However, IMPATT devices are more efficient and have higher output power than Gunn devices making them a good choice for power sources in solid-state transmitters. Both devices may be phase-locked to stabilize the output frequency and reduce FM noise.

Figure 8.11 shows the state-of-the art in power output for commercially available Gunn and IMPATT diodes as a function of frequency in 1987. This figure also gives peak output power for IMPATT

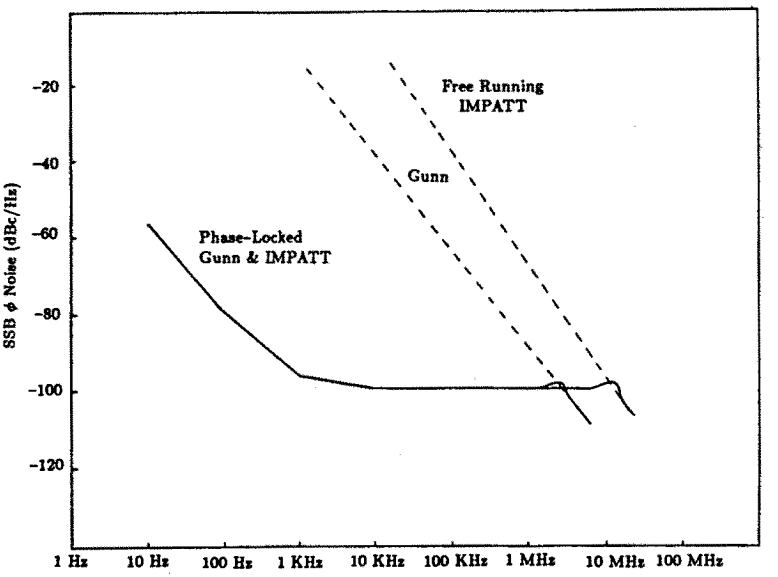

Figure 8.12 SSB phase noise spectrum for locked and unlocked Gunn and IMPATT diodes.

diodes under pulsed conditions (Hughes, 1987). A comparison of RMS phase noise characteristics is shown in Fig. 8.12 for locked and unlocked Gunn and IMPATT sources. Short-term variations in local oscillator phase can adversely affect measurements in a polarimetric radar system. Therefore, it is necessary to quantify this error before specifying a particular device. Following an analysis by Cutler and Searle [1966], the RMS phase error of the oscillator voltage may be related to the single side-band phase noise spectrum, $S_\phi(f)$, by

$$\phi_{rms} = \sqrt{2 \int_{f_{\min}}^{\infty} S_\phi(f) df} \tag{3.1}$$

The lower limit of integration, $f_{\min}$, is given by T_d^{-1} where T_d is the time delay between consecutive measurements. Since phase noise characteristics are usually published by the manufacturer, (3.1) is a convenient formula for computing RMS phase error and is useful for estimating the contribution of LO noise to the total system phase error.

Two-terminal devices such as the above diodes can be used as amplifiers when connected as shown in Fig. 8.13. This technique, known

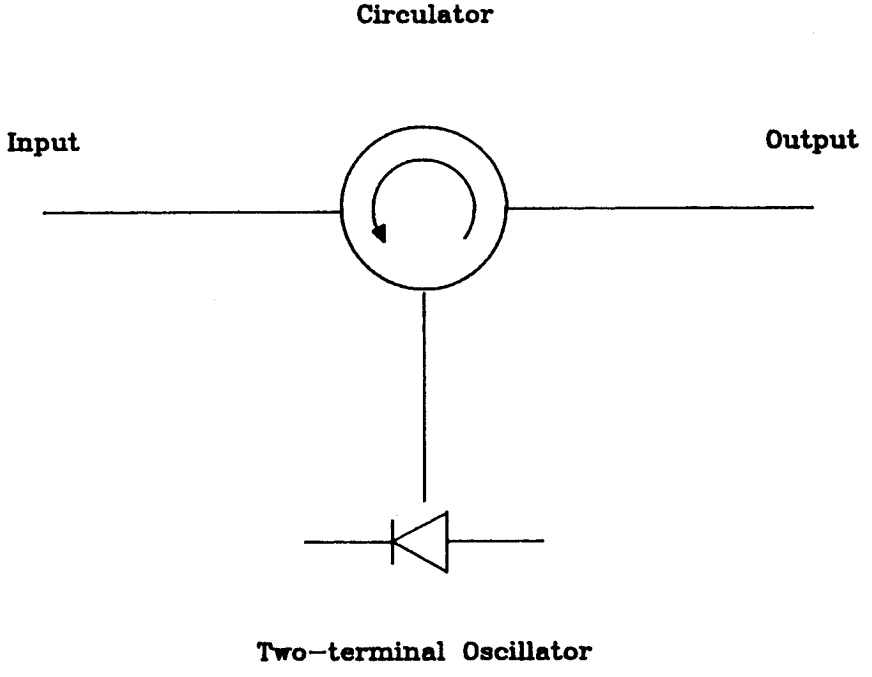

Figure 8.13 Reflection amplification with two terminal devices.

as reflection amplification, may be used either in a stable, nearly linear mode, or in an unstable, injection-locked mode. In both cases these devices may be operated as either CW or pulsed amplifiers. In the case of the stable amplifier mode, the load impedance is adjusted to be greater than the negative impedance of the device. When no drive signal is present, the output signal is zero. In the case of injection locking, the circuit impedance is lower than the negative impedance of the device and the circuit will oscillate with no input signal present. With sufficient drive power, the output signal will track the phase of the input. Therefore, a high power, low phase-noise transmit signal may be achieved by driving such an amplifier with a phase-locked source.

Another common method of obtaining greater output power is to combine the output of two or more devices. This may either be done on the circuit level, combining several devices in a resonant cavity,

or on the module level, combining packaged devices with an external network. The individual oscillators are phase-locked with an injecting signal to give maximum combining efficiency. Hughes [1987, p. 46] reports a 26-way combiner operating at 44 GHz with better than 90 percent combining efficiency. A pulsed amplifier combining the output of 4 diodes at 95 GHz and generating a peak-power output of 40 W with 43 dB of gain is also available from Hughes [1987, p. 48].

Frequency multipliers

Frequency multipliers are also employed in millimeter-wave systems and test equipment as an inexpensive method of obtaining power levels of several milliwatts. For example, a broad band frequency multiplier may be added to a microwave sweeper to implement a full waveguide band millimeter-wave source. Currently available doublers have efficiencies of between 5 and 30 percent and may provide tens of milliwatts of output, which is sufficient for local oscillators, network measurements and short range scattering studies. Triplers and quadruplers are generally less efficient but may be required depending on the available driving source and desired output frequency [Millitech, 1987, p. 3–25].

c. High Power Oscillators

Microwave oscillators such as the magnetron and reflex klystron have been successfully extended into the millimeter-wave region although power output falls off rapidly with increasing frequency in both cases. For these tubes, the resonant structure that determines the operating frequency of the device also serves as the electron beam collector and therefore must dissipate a significant amount of heat. These structures become more and more delicate as frequency increases, eventually limiting the maximum output power and lifetime of the tube. Practical magnetrons are therefore limited to about 100 GHz, with relatively short lifetimes (approximately 1000 h). Reflex klystrons, on the other hand, have been employed as local oscillators at frequencies up to 220 GHz.

The Extended Interaction Oscillator, (EIO), although requiring a delicate resonant structure to modulate the electron beam, employs a separate collector and is thus capable of relatively large output power and long life. The EIO is commercially available and provides mod-

erate amounts of power across the millimeter-wave region (1.5 kW peak at 95 GHz, 70 W peak at 220 GHz). These tubes are inherently narrow-band (.5 percent) although a certain amount of mechanical and electrical tuning is possible. Grid controlled versions are available which are driven by low-power, compact modulators making the EIO a good choice for portable radar systems. The Backward Wave Oscillator (BWO) or carcinotron also employs a separate collector but achieves much broader bandwidth than the EIO (approximately 10 percent) by employing a slow-wave structure instead of a fixed resonant cavity. The BWO is tuned by varying the electron beam voltage and may be phase-locked to an external reference. As early as 1961, the Compagnie générale de télégraphie Sans Fil (C.S.F.) of France had produced a 140 GHz BWO that produced more than one watt of output power [Covert, 1961; Meredith, 1963, p. 404].

Millimeter-wave devices that do not depend upon the interaction of the electron beam with physical structures, such as the gyrotron and Relativistic Electron-Beam (REB) devices are capable of hundreds of kilowatts of pulsed output power. Because of the large cavity dimensions, severe multimoding may occur in the gyrotron. The main interest to date in gyrotrons has been their application to plasma heating problems where signal purity is of little concern. The REB requires extremely high accelerating potentials (1MV) and thus is limited to laboratory applications at the present time.

d. High Power Amplifiers

A commonly used high power millimeter-wave amplifier is the Travelling Wave Tube (TWT) amplifier. The TWT employs a slow-wave structure for interaction between the electron beam and the input field. This structure has the form of a either a helix or a periodic coupled-cavity. Difficulties in cooling the helix structure, especially at millimeter-wavelengths, has led to the widespread use of the coupled-cavity approach for most high power and short wavelength applications. Coupled-cavity TWTs have bandwidths up to approximately 5 percent, and are available for either pulsed or CW operation up to about 100 GHz. TWTs usually require well-regulated high-energy power supplies. These may exceed the cost of the tube itself and their size and power consumption may prohibit the use of TWTs in certain portable applications.

Another amplifier available for millimeter-wave frequencies up to

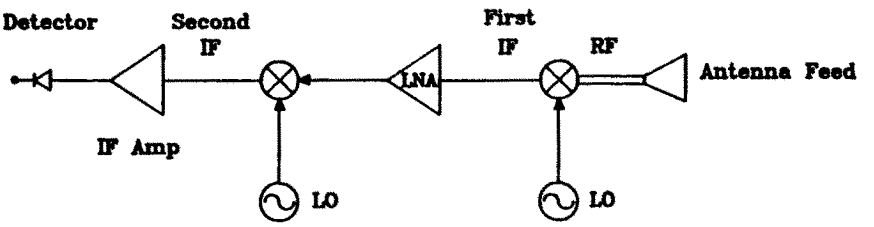

Figure 8.14 Basic millimeter-wave receiver employing first stage down-converter.

100 GHz is the Extended Interaction Amplifier (EIA). Because it employs a periodic resonant structure, it is inherently narrow band (.2 percent) although some mechanical tuning is possible (.5 percent). Like the EIO, the EIA may employ a grid controlled beam, thus significantly reducing the modulator and power supply requirements.

e. Receiver Front-End Design

Millimeter-wave receivers have historically employed a down- converter as a first stage followed by a microwave Low Noise Amplifier (LNA). In recent years, however, three terminal devices have been developed for use at millimeter-wavelengths having noise temperatures competitive with mixer techniques. HEMT or High Electron Mobility Transistor devices have been employed in amplifiers at frequencies up to 95 GHz yielding impressive noise temperatures in cryogenic and room temperature LNAs.

Downconversion techniques

The basic configuration of a millimeter-wavelength receiver is shown in Fig. 8.14. To a first approximation the noise figure of this receiver, F_{rec}, is given by

$$F_{rec}(dB) = L_{antenna}(dB) + L_{mixer}(dB) + F_{lna}(dB) \qquad (3.2)$$

where $L_{antenna}$ is the antenna + waveguide loss before the mixer, L_{mixer} is the mixer conversion loss and F_{lna} is the noise figure of the

LNA. Typical values for L_{mixer} are between 4 and 10 dB for state-of-the-art Schottky diode mixers, depending on the frequency of the detected signal. In most applications, it is convenient to downconvert to frequencies between 160 MHz and 2 GHz where LNAs are available having noise figures around 1 dB. Thus the receiver noise figure is primarily determined by the conversion loss of the millimeter-wave mixer. There are several common types of low-conversion loss mixers used in millimeter-wave receivers most employing GaAs Schottky-barrier beam-lead or whisker-contacted diodes. The simplest of these devices is the single-ended mixer shown in Fig. 8.15. Single-ended mixers require the least amount of LO drive (about 1 mW) but a means of diplexing the LO with the signal must be provided. The simplest technique is to inject the LO signal via a directional coupler, although this may contribute significantly to overall conversion loss, especially above 100 GHz where waveguide components are very lossy. Another option is to use quasi-optical injection as diagrammed in Fig. 8.16. A Fabry-Perot interferometer having high transmissivity at the RF frequency and high reflectivity at the LO frequency is used to combine the signal and local oscillator [Predmore, et al. 1985]. Although this method of LO injection is considerably more costly, insertion loss may be reduced from 1 or 2 dB in the case of the coupler to several tenths of dB using optical techniques.

An attractive option to the single-ended mixer is the *harmonic* or *sub-harmonic* mixer. While harmonic instrumentation mixers typically have 20 to 50 dB conversion loss and operate on any one of many harmonics, harmonic mixers optimized to employ a specific sub-harmonic (usually 2 to 4) offer conversion loss which is competitive with fundamental mixers. Harmonic mixers received considerable attention during the 60's and 70's when sufficient fundamental LO drive was difficult to achieve [Meredith, 1963; Cohn, 1975]. The problem of diplexing the signal and LO is avoided by using a crossed-waveguide configuration to inject the half or quarter frequency LO. Excellent LO to RF isolation is achieved because the RF waveguide is cut-off at the LO frequency. Although considerably more LO drive is required to pump harmonic mixers (approximately + 6 dBm), the cost of achieving this level at one-half or one-quarter the signal frequency is likely to be cheaper than providing less LO power to drive a fundamental mixer, especially for signals above 100 GHz.

Another device providing separate LO and RF ports is the single-

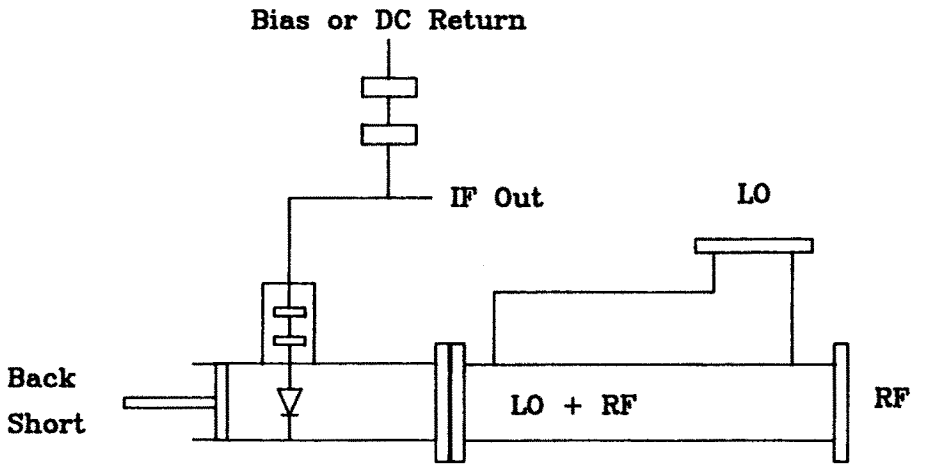

Figure 8.15 Single-ended mixer showing directional coupler used as LO-RF diplexer.

balanced mixer. This mixer employs two diodes and requires considerably more LO drive (+10 dBm) than single diode mixers. Other advantages of the single-balanced mixer are its high LO-RF isolation, LO noise supression and intermodulation supression. Single-balanced mixers are commercially available to 110 GHz [Millitech, 1986, p. 2–5; Hughes, 1987, p. 90].

Very low noise temperatures have been achieved using superconductor-insulator-superconductor (SIS) mixers cooled to 4 K. These devices have been primarily developed for use in radio telescopes which usually employ cryogenic front ends, but may become of greater interest to other users as superconductor technology progresses to higher temperatures. A single-ended mixer employing an SIS junction was described by Pan (1988) which had a noise temperature of 46 K ± 6 K between 88 and 115 GHz.

f. Three-Terminal Low Noise Amplifiers

The majority of low noise amplifiers in the upper microwave region employ GaAs Field Effect Transistor (FET) devices at the present time. Packaged LNAs are currently available to 45 GHz (F = 8 dB, Avantek)

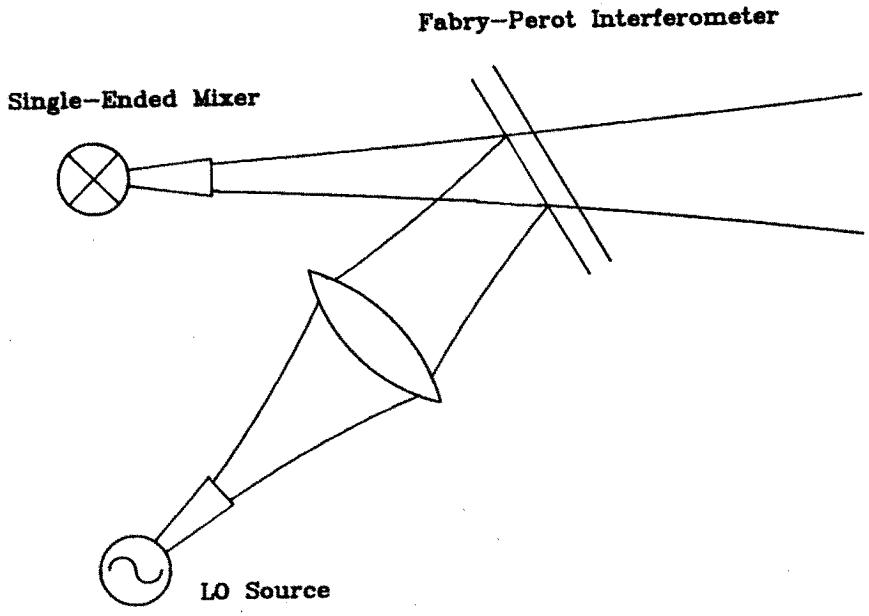

Figure 8.16 Single-ended mixer using quasi-optical LO injection.

employing GaAs FET amplifiers. Recent research on millimeter-wave LNAs has focused on the High Electron Mobility Transistor (HEMT). Multistage cryogenic HEMT LNAs operating at 43 GHz have been reported with an overall system noise temperature of 105 K (Weinreb, 1988). HEMT amplifiers have been extended to higher frequencies, although gain and noise figure degrade roughly as f^{-1}.

g. Waveguide Components

Standard waveguide is available throughout the millimeter-wave region. The various waveguide bands are listed in Table 8.1 together with the EIA waveguide designation, frequency range, dimensions and range of attenuation for silver-plated waveguide. Most common microwave devices, including switches, circulators, isolators, etc., are available in waveguide up to W-Band, and with some limitations to G-band. Due to the high loss in waveguide at W, F and G-band it is advisable to avoid any configuration requiring waveguide runs over a few centimeters.

(a)	(b)	(c)	(d)	(e)	(f)
Ka	WR–28	26.5–40	.72–.49	.711 × .356	.914 × .559
Q	WR–22	33–50	1.02–.69	.570 × .280	.772 × .488
U	WR–19	40–60	—	.480 × .240	.681 × .442
V	WR–15	50–75	1.74–1.28	.380 × .190	.579 × .391
E	WR–12	60–90	3.06–1.71	.310 × .150	.513 × .356
W	WR–10	75–110	—	.254 × .127	.458 × .330
F	WR–8	90–140	4.99–3.25	.232 × .102	.406 × .305
D	WR–6	110–170	12.60–8.33	.170 × .083	.368 × .286
G	WR–5	140–220	16.80–11.42	.130 × .065	.333 × .268

Table 8.1 Waveguide bands. (a) Waveguide band designation; (b) EIA waveguide designation; (c) Frequency range in GHz; (d) Range of attenuation, lowest to highest frequency, in $dB \cdot m^{-1}$; (e) Inside dimensions $a \times b$, in cm; (f) Outside dimensions $a \times b$, in cm.

Quasi-optical techniques are especially attractive for polarimetric radars, where substantial manipulation of the radiated signal is necessary. Millimeter-waves are launched along the axis of the quasi-optical guide using a scalar-feed horn which radiates a beam with an axial-symmetric amplitude distribution. Periodic lens are used to confine the energy to a well defined beam. Because no currents are excited on metallic surfaces as in waveguide, quasi-optical guides are much more efficient. Other quasi-optical devices that are useful in polarimetric radars include quarter and half-wave plates, wire-grid polarization splitters and lens antennas. The 225 GHz polarimeter described in section 6 makes use of several of these devices.

8.4 Error Analysis

When studying possible error sources in polarimetric measurements, it is helpful to separate fixed and randomly varying errors. The effects of fixed errors, such as phase imbalance between orthogonal receive channels, or antenna imperfections can be calibrated out periodically. Slowly varying fluctuations in phase and amplitude due to temperature changes or aging may also be treated as fixed errors as long as the changes are slight between calibrations. Random errors along with rapidly fluctuating non-random errors may not be removed by calibration techniques and their effects will add errors to the measurements. However, the effects of random errors may often be reduced by averaging.

A particular concern at millimeter-wavelengths is the phase stability of both transmitter and receiver. Phase errors due to oscillator phase noise and physical variations in the radar dimensions scale with frequency and are therefore greater for millimeter-wave radars than for their microwave counterparts. Signal fading rate also scales with frequency making the millimeter radar more sensitive to changes in the targets range and orientation range than microwave radars. In this section, the effects of random and rapidly fluctuating non-random errors are considered.

Random or quasi-random errors in the measured complex voltage can be treated as independent fluctuations in the phase and magnitude of the signal. Phase error sources include phase noise of the reference oscillator, random motion between the radar and the target, atmospheric anistropy, and thermal and quantization noise in the receiver. Errors in the measured magnitude of the signal may also be caused by receiver thermal and quantization noise, and atmospheric turbulence, anistropy and loss fluctuations due to changes in water vapor and hydrometeor density. These error sources are analyzed separately below.

a. Propagation Considerations

a.1 Attenuation by water vapor

Several algorithms based on theoretical analysis and empirical observations have been developed [Van Vleck, 1957; Waters, 1976] to estimate propagation losses due to water vapor under given conditions of temperature, pressure, water content and particulate distributions, the most extensive by Liebe [1985]. While loss due to water vapor rarely reaches 1 $dB \cdot km^{-1}$ at 35 GHz, attenuation can be as high as 3 $dB \cdot km^{-1}$ at 95 GHz and greater than 10 $dB \cdot km^{-1}$ in the 220 GHz window. Under cool, dry conditions, however, this loss drops to insignificant levels at 35 GHz while only reaching .5 to 1 $dB \cdot km^{-1}$ at 220 GHz. Thus, depending on prevailing weather conditions, operation over ranges of several kilometers may or may not be severely affected.

a.2 Attenuation and scattering by liquid water

Estimates of loss due to liquid water, appearing as rain, fog or clouds may be carried out using Mie scattering theory [1908] and an appropriate drop size distribution. A thorough treatment of this pro-

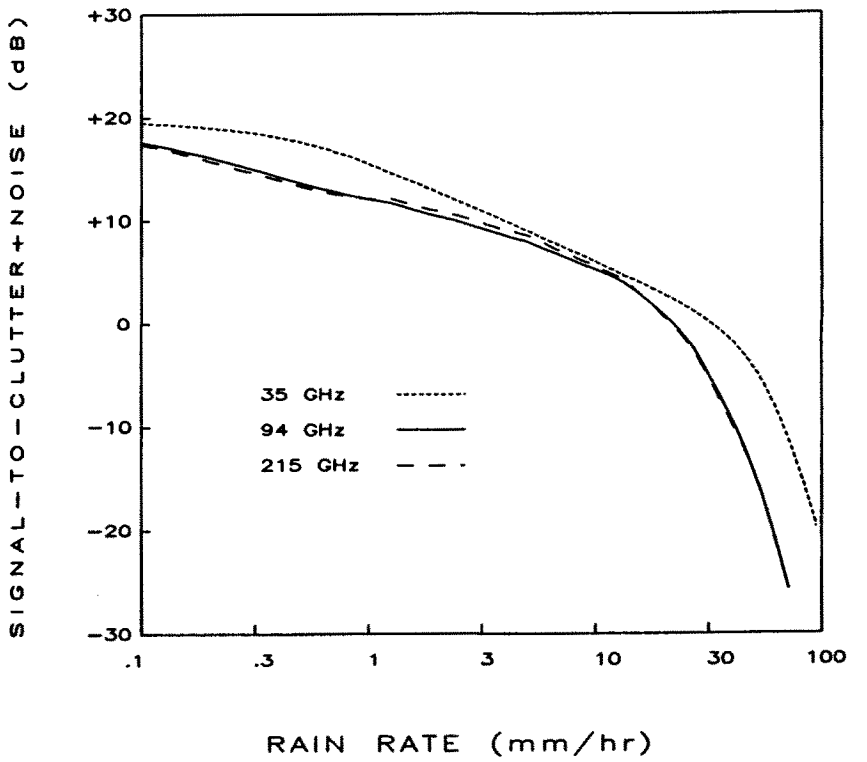

Figure 8.17 Signal-to-clutter plus noise versus rain rate for 35, 94 and 215 GHz.

cedure is given in Ulaby et al. [1981]. The volume backscattering coefficient may also be computed in this way. As an example, consider a radar illuminating a surface with $\sigma^\circ = -10$ dB. The radar is 1 km from the target and the radar signal propagates through rain. Because the signal is degraded both by attenuation and volume backscatter from the rain, degradation may be measured by evaluating the ratio of desired signal power to the sum of thermal noise power and clutter (i.e., backscatter from rain) power. Figure 8.17 compares the signal-to-clutter+noise ratio for rainfall rates between .1 and 100 mm/hr for radars operating at 35, 95 and 215 GHz. All three radars have a clear-air signal-to-noise ratio of 20 dB for comparison. Because most raindrops are larger than the Rayleigh limit ($.08\lambda - .10\lambda$) for the three frequencies, the amount of attenuation and backscatter in rain is seen to be only weakly dependent on frequency.

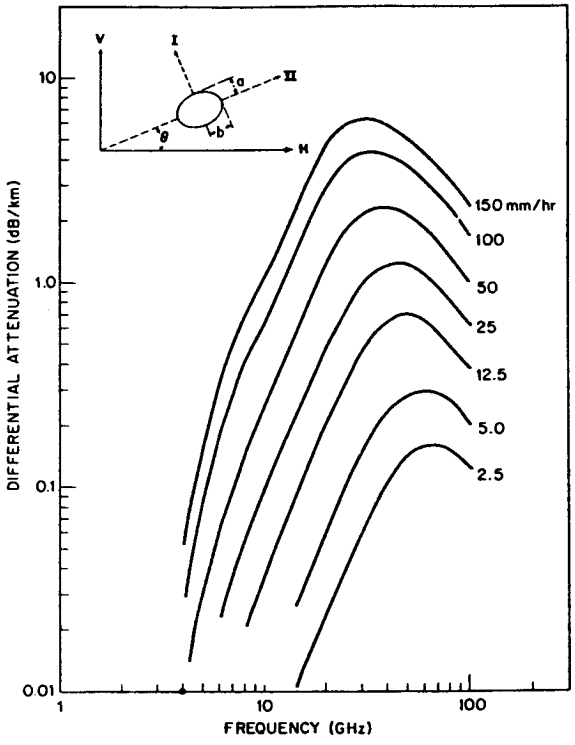

Figure 8.18 Rain-induced differential attenuation between polarizations I and II for various rain rates (Morrison and Chu, 1973).

a.3 Propagation in anisotropic media

A wave propagating in an anisotropic medium whose slow or fast axis is not aligned with the polarization vector will undergo a transformation from its original polarization state to another. Under controlled conditions this property is useful in generating elliptical polarizations from a linearly polarized wave and vice versa. However, for a polarimetric radar operating in random anisotropic media the polarization state of both the transmitted and scattered waves will fluctuate randomly.

Several authors [Morrison, 1973; Oguchi, 1975; Hogg, 1975; Cox, 1979] have discussed wave depolarization for propagation through rain cells. Although rain drops are often modeled as spheres, the shapes of larger drops are better approximated by oblate spheroids that scatter

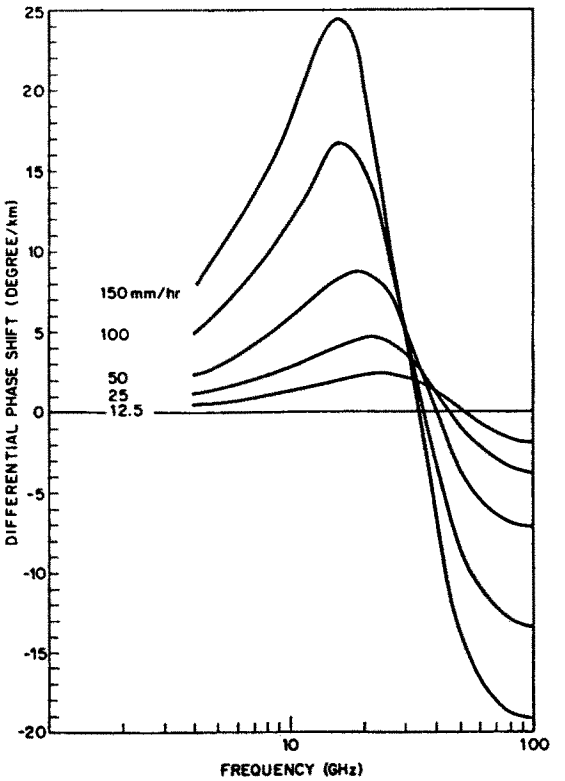

Figure 8.19 Rain-induced differential phase shift between polarizations I and II for various rain rates (Morrison and Chu, 1973).

and absorb polarization parallel to the major and minor axes differently. Morrison [1973] used perturbation techniques to compute differential attenuation and phase shift between polarizations aligned parallel and perpendicular to the major axis of rain drops as shown in Figs. 18 and 19 between 1 and 100 GHz. In Fig. 8.20, cross polarization discrimination (i.e., the ratio of co-to-cross-polarized power) is plotted as a function of horizontal polarization attenuation at 11, 17.71 and 60 GHz [Hogg, 1975], showing a decrease in slope for the higher frequency. This trend is due to small, nearly spherical drops attenuating the transmitted signal at higher frequencies, whereas attenuation at low frequencies is due to large, non-spherical drops that depolarize more strongly.

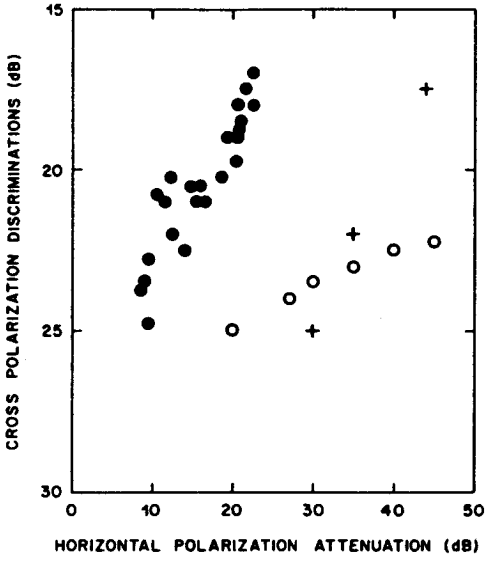

Figure 8.20 Measured rain-induced cross polarization for horizontal polarization transmitted; ··· 11 GHz, +++ 17.71 GHz, ○○○ 60 GHz [Hogg and Chu, 1975].

a.4 Atmospheric turbulence

Fluctuations in amplitude and angle of arrival are known to be caused by atmospheric turbulence. Theoretical models first developed by Chernov [1960], and Tatarski [1961] in the Soviet Union, and later by Clifford [1970] depend on the temperature and humidity structure parameters C_T and C_ρ. C_T may be found by measuring the mean square temperature variation between two points separated by a distance d,

$$C_T = \langle (T(0) - T(d))^2 \rangle d^{-2/3} \qquad {}^\circ C^2 m^{-2/3} \tag{4.1}$$

Similarly, C_ρ is given by

$$C_\rho = \langle (\rho(0) - \rho(d))^2 \rangle d^{-2/3} \qquad (gm^{-3})^2 m^{-2/3} \tag{4.2}$$

where ρ is water vapor density in grams m^{-3}. McMillian and Wiltse [1979] presented measured and computed values for peak-to-peak fluctuations of 95 and 140 GHz signal amplitude versus C_T^2 for a two kilometer path. The 95 GHz data are given in Fig. 8.21 and indicate

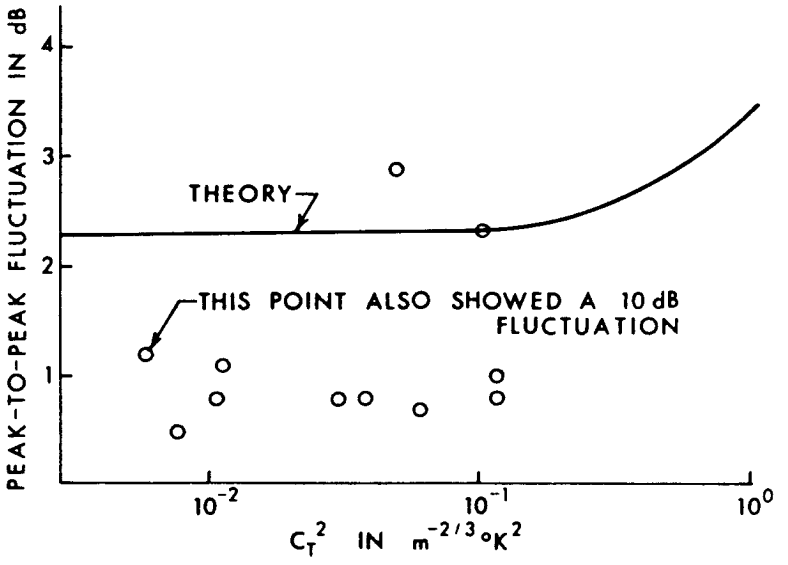

Figure 8.21 Peak-to-peak fluctuations versus C_T^2 at 94 GHz. Values of parameters used for calculation are as follows: $L_0 = 1.5$ m, $T = 288.8$ K, $\rho = 8.5$ gm^3, and $C_\rho = 1.45\times10^4 m^{-1/3}$g/m^3. Measured results are shown as circles [McMillan and Wiltse, 1979].

that fluctuations of several dB·km^{-1} may be expected under typical atmospheric conditions. In Fig. 8.21, L_o is the outer scale dimension of the turbulent cell.

b. Oscillator Phase Noise

The reference phase-locked oscillator (PLO) shown in Fig. 8.3 serves as a common source both for the transmitted wave and the receiver LO and acts as a phase memory device. The oscillator output may be expressed mathematically by

$$V_{PLO} = V_0 \cos(\omega t + \phi(t)) \tag{4.3}$$

where $\phi(t)$ is a randomly varying phase term. To quantify the error due to $\phi(t)$ it is useful to compute the rms value of the deviation of $\phi(t)$ around some mean value. The rms phase noise may be found from (3.1) and the power spectral density of V_{PLO} (assuming V_0 is constant)

where

$$S_\phi(f) = S_{PLO}(f)/P_{carrier} \tag{4.4}$$

and $f_{\min}$ in (3.1) is the frequency below which fluctuations will not affect the measurements. In the case of a polarimetric radar, fluctuations in V_{PLO} that occur between transmission and reception affect the measured phase. Thus $f_{\min} \leq \frac{C}{2 \cdot R}$, where R is the range to the target, and c is the speed of light. As the off-diagonal terms of the scattering matrix are equal for stationary targets, it is not necessary that phase stability be maintained during the period between orthogonal transmit pulses. Phase-locked oscillators are commonly characterized by a single-sideband phase-noise diagram. Figure 8.22 shows a typical 94 GHz SSB phase-noise diagram for a Hughes PLO [Hughes, 1987, p. 47]. By integrating the phase noise spectrum from $f_{\min}$ to infinity, the rms phase noise may be plotted as a function of range as given by Fig. 8.23. The dashed line shows rms phase noise for a free running oscillator. This analysis indicates that a free running oscillator can be used for short range applications, although the inherent frequency drift of non-locked sources is undesirable in most applications.

b.1 Thermal noise

Another important source of random phase and amplitude errors in radar measurements is receiver thermal noise. Figure 8.24 shows the desired signal phasor, V_s, and the additive random noise phasor, V_n. Assuming the distribution of the magnitude of V_n is Rayleigh and the phase has a uniform distribution, the rms value of $\delta\phi_n$ is given by Viterbi [1966] as a function of signal-to-noise power. This result is given in Fig. 8.25 which indicates that significant phase errors occur for signal-to-noise ratios (SNR) below 30 dB. The error in the magnitude of V_s is given by

$$\frac{\sigma_v}{V_s} = \sqrt{SNR} \tag{4.5}$$

where σ_v is the RMS noise voltage. In both cases, the signal-to-noise ratio may be increased by averaging N correlated samples. For coherent systems, the SNR improves in proportion to N; the SNR improves in proportion to the square root of N for incoherent systems.

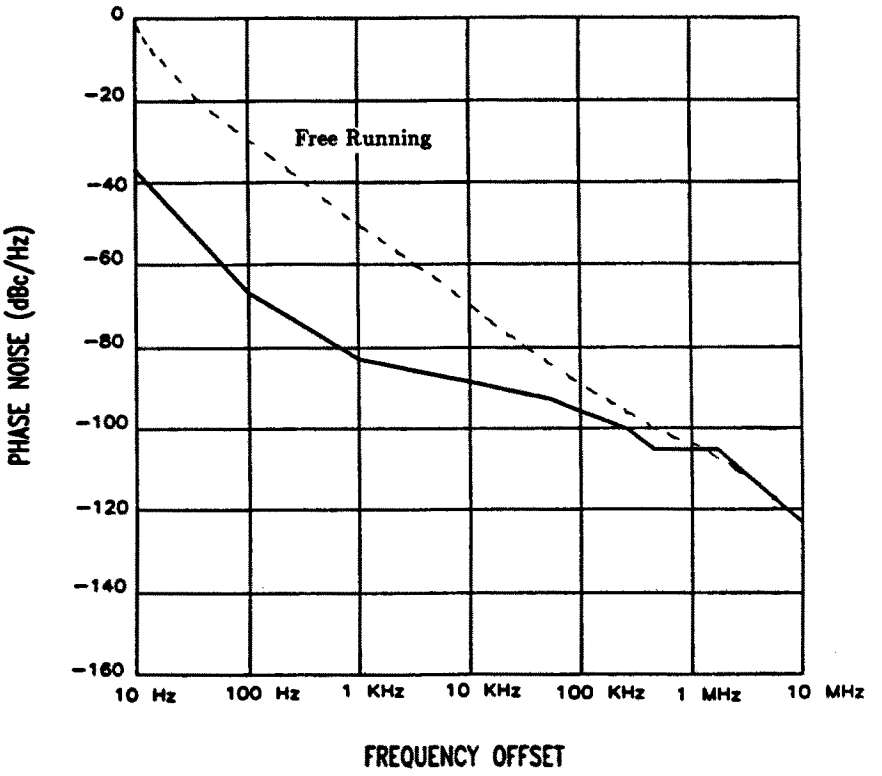

Figure 8.22 SSB ϕ noise of 95 GHz phase-locked Gunn (——). Free running oscillator, (- - - - - -).

b.2 Mechanical vibrations

Phase errors may also be contributed by mechanical vibrations of the radar. The two-way electrical path length of the radar signal is given by

$$\phi_r = \phi_0 + \Delta\phi_v = \phi_0 + 4\pi r(t)/\lambda \tag{4.6}$$

where $r(t)$ is the mechanical deflection of the radar's position in the direction of the target about its mean position. Assuming simple har-

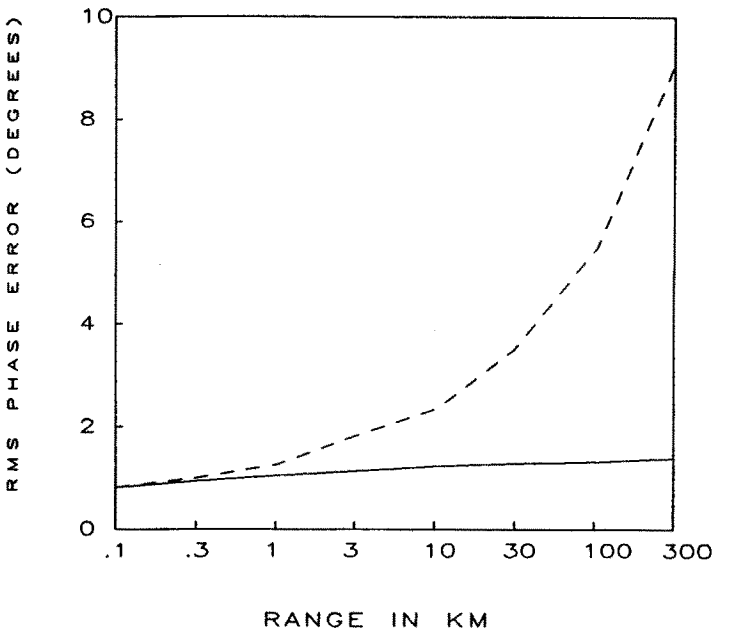

Figure 8.23 RMS phase error as a function of range equivalent time delay, (——). Free running 95 GHz oscillator, (- - - - - -).

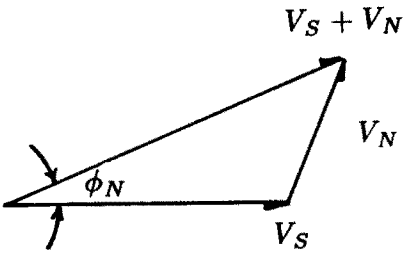

Figure 8.24 Phase error, ϕ_N, generated by noise voltage, V_N.

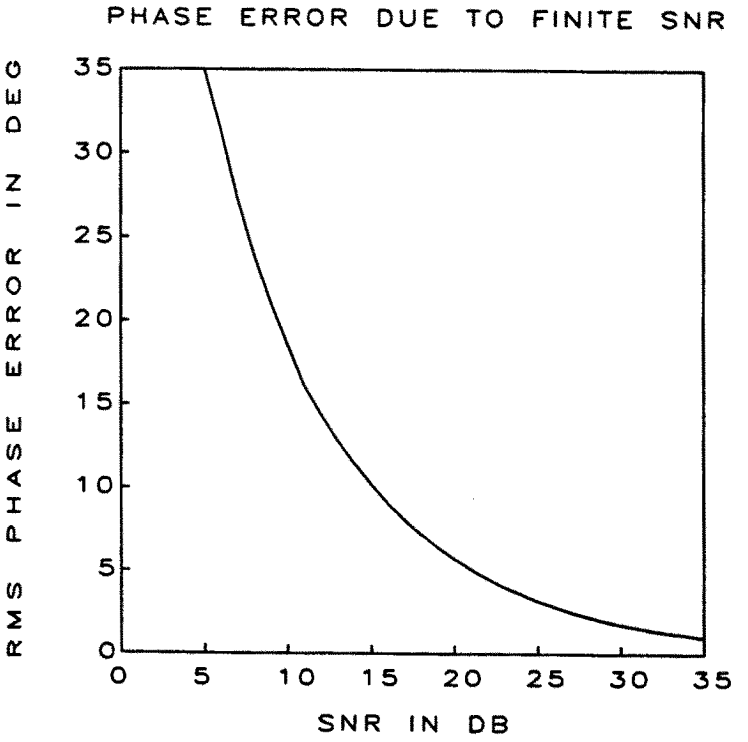

Figure 8.25 RMS phase error as a function of signal-to-noise ratio.

monic motion, $r(t) = \Delta R \sin 2\pi f_v t$, where the vibration frequency is given by f_v and the deflection magnitude is given by ΔR. The mechanical acceleration of the radar is $\ddot{r}(t) = -(2\pi f_v)^2 \Delta R \sin 2\pi f_v t$ so the deflection magnitude can be expressed

$$\Delta R(f) = \frac{a(f)}{4\pi^2 f_v^2} \tag{4.7}$$

where $a(f)$ is the acceleration spectrum in ms^{-2}. In order that phase errors due to vibrations be maintained below some value, $\Delta\phi_v$, the following condition must be satisfied

$$\Delta\phi_v > \frac{4\pi r(t)_{\max}}{\lambda} = \frac{a(f)}{\pi f_v^2 \lambda}$$

or

$$a(f) < \pi\lambda f_v^2 \Delta\phi_v \qquad m \cdot s^{-2} \tag{4.8}$$

Typical vibrational spectra are confined to frequencies below 1 KHz. For $\lambda = 3.2$ mm (95 GHz) and $\Delta\phi_v = 1°$ (.0174 rad), the acceleration must be less than .36 g at 100 Hz and less than 2.23 g at 250 Hz. Therefore, typical vibrations should not contribute appreciable phase errors so long as polarimetric measurements are made at pulse repetition frequencies (PRF) above 1 KHz.

A similar analysis holds for relative harmonic motion between the H and V channels of the polarimeter. In that case, the phase error, $\Delta\phi_{rel} = 2\pi\Delta x/\lambda$, where Δx is the relative path lengths between channels. In this case, sampling the signal at 1 KHz should also cause rms phase errors due to this effect to be negligible.

b.3 Temperature effects

Slow changes in the path length between H and V channels can contribute errors to polarimetric data. Temperature changes will contribute a relative phase error,

$$\Delta\phi_T = \frac{2\pi}{\lambda} K_T \Delta T \Delta L \tag{4.9}$$

where K_T is the linear thermal expansion coefficient, ΔT is the temperature change and ΔL is the path length difference between the H and V channels. For $\Delta L = n\lambda$, $\Delta\phi_T/\Delta T = 6.1\times10^{-3}n$ degrees/°C for copper waveguide. Thus, the phase error $\Delta\phi_T$ due to temperature variations of 10°C or less will be negligible if the path length difference is small ($n < 10$). Temperature variations of less than 10°C are easily achieved by thermally stabilizing the radar system with controlled heating elements.

Additional phase and amplitude variations due to changes in temperature will occur within individual components in the transmitter and receiver. This error may be quantified by the radar system designer by combining the errors in each component as specified by the manufacturer. Proper temperature stabilization of the instrument will greatly reduce the effects of ambient temperature variations and will reduce the need for frequent calibration. In general, variations due to temperature changes will not vary randomly during a given measurement, but will be some complex function of the temperature distribution within

the instrument. Thus, errors due to temperature fluctuations can not be reduced by signal integration. In cases where many independent measurements of the target are used to reduce random errors, errors due to uncalibrated system drift will become more significant.

b.4 Quantization errors

Errors due to quantization of received signals by A/D converters may be significant, especially for wide dynamic range systems. Voltage quantization error is given by:

$$(V_{\max} - V_{\min})/2^{N_{bits}} \tag{4.10}$$

where V is a voltage derived from linear, square law or log detection of the signal. For example, an 80 dB dynamic range log detector has a voltage swing of 0 to 2 volts at its output, corresponding to 25 mV·dB^{-1}. An 8 bit A/D converter results in a voltage quantization error of 2V/256 =7.8 mV or .31 dB.

The phase difference between two signals, i.e. the phase reference signal and the down-converted radar return, is usually measured using an inphase/quadrature (I/Q) detector. For an ideal I/Q detector, the angle between the two input signals is given by $\theta = \arctan(V_Q/V_I)$. The voltage, V_I, at the output of the in-phase (I) channel and V_Q at the output of the quadrature (Q) channel will vary between $-V_{\max}$ and $+V_{\max}$. If S_I is the digital word representing V_I and S_Q is the digital word representing V_Q, the quantization of θ is given by

$$\begin{aligned} \delta\theta/\delta S_I &= -V_Q/(V_{\max}2^{N-1}) \text{ radians} \\ \delta\theta/\delta S_Q &= V_I/(V_{\max}2^{N-1}) \text{ radians} \end{aligned} \tag{4.11}$$

For an 8 bit A/D converter, the maximum quantization error in θ is $1/128 = .008$ radians or .45 degrees. Taking the average of N independent samples of time varying signals may be used to reduce quantization error by a factor of N (coherent integration) or $\sqrt{(N)}$ (incoherent integration) so long as the standard deviation of the signal voltage is large compared to the least significant bit quantization level (Ruf, 1988).

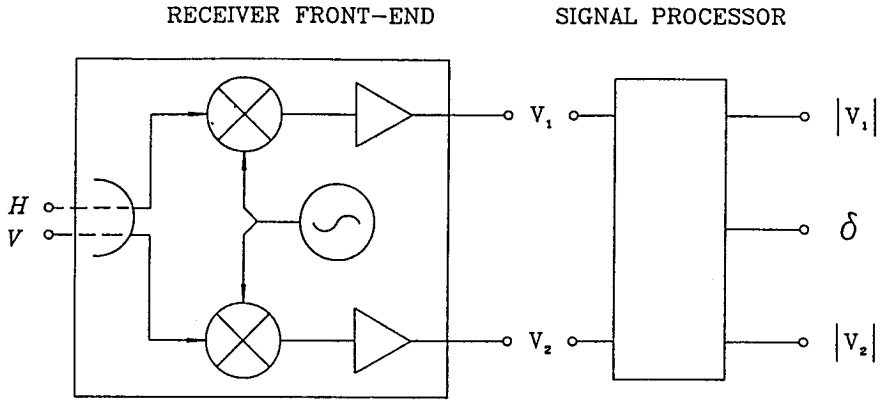

Figure 8.26 Receiver front end and signal processor.

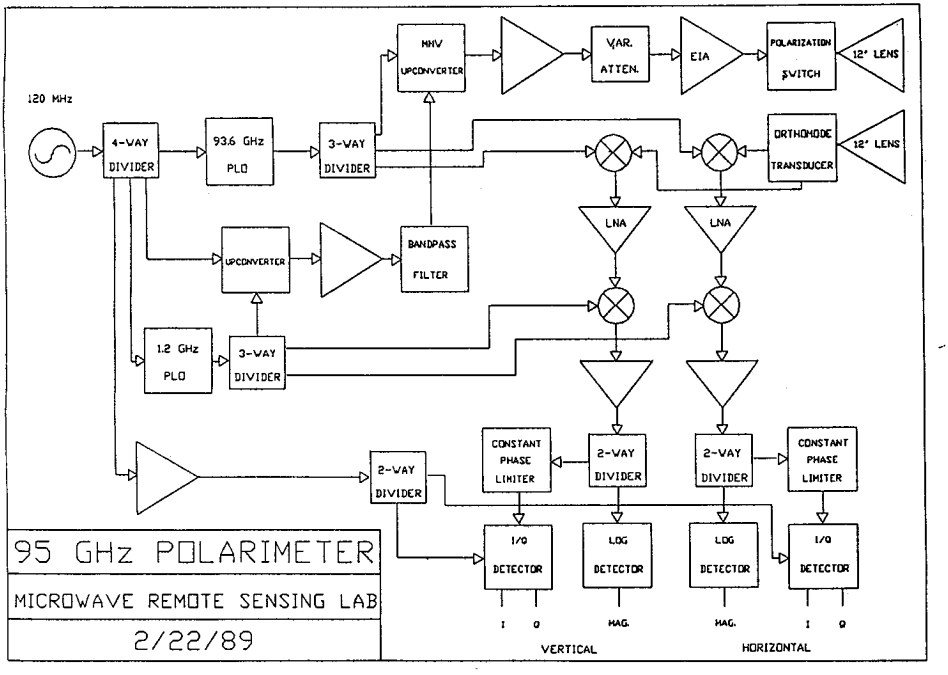

Figure 8.27 95 GHz polarimeter radar block diagram.

b.5 Combined phase error

The combined phase error due to all random and rapidly varying sources may be found by taking the root sum square of the individual standard deviations

$$\sigma_{RMS} = \sqrt{\sigma_{PLO}^2 + \sigma_{A/D}^2 + \sigma_N^2 + \sigma_T^2 + \sigma_{AT}^2 + \sigma_M^2} \tag{4.12}$$

where

σ_{PLO} = rms phase error of PLO
$\sigma_{A/D}$ = rms phase error due to quantization
σ_N = rms phase error due to thermal noise
σ_T = rms phase error due to random temperature variations
σ_{AT} = rms phase error due to atmospheric effects
σ_M = rms phase error due to mechanical vibrations

The total random amplitude error may be computed in a similar fashion, combining the effects of thermal noise, quantization error, temperature and turbulence.

8.5 Receiver Front-End and Transmit Polarization Calibration

Calibration of an incoherent polarimeter has been described previously by Wood [1986]. Wood's procedure involves using four in-scene reflectors, three of which scatter waves having known polarization and the fourth being an odd-bounce reflector, such as a trihedral corner reflector. Fixed errors are removed from the receiver so it may accurately measure the polarization state of an incoming wave, and then the calibrated receiver is used to measure the state of the four transmitted polarizations used in making Stokes matrix measurements. An alternate technique, which is particularly well-suited to millimeter-wave systems having small antennas, is to use a single corner reflector and a rotating polarizer placed in front of the receiver antenna. This technique simplifies field measurements and eliminates errors that arise from clutter in the return signal from an in-scene reflector.

Figure 8.26 is a simplified schematic of the receiver front-end. The input wave may be described by a 2×1 (Jones) vector $[H, V]^T$ where H and V are the horizontal and vertical components of the received wave and T indicates the transpose of the row matrix. Similarly, $[V_1, V_2]^T$ represents the output voltages of the nominally orthogonal IF ports.

To account for phase and amplitude imbalance in the LO branches, mixers and LNAs, as well as gain imbalance and imperfect polarization separation in the antenna, the input field vector can be related to the output voltage vector by a 2×2 matrix,

$$\begin{bmatrix} V_1 \\ V_2 \end{bmatrix} = \begin{bmatrix} a_1 & b_1 \\ c_1 & d_1 \end{bmatrix} \begin{bmatrix} H \\ V \end{bmatrix} = a_1 \begin{bmatrix} 1 & A \\ B & C \end{bmatrix} \begin{bmatrix} H \\ V \end{bmatrix} \tag{5.1}$$

where $A = b_1/a_1$, $B = c_1/a_1$ and $C = d_1/a_1$. Solving for H and V in terms of V_1 and V_2 yields

$$\begin{bmatrix} H \\ V \end{bmatrix} = \frac{1}{a_1(C - AB)} \begin{bmatrix} C & -A \\ -B & 1 \end{bmatrix} \begin{bmatrix} V_1 \\ V_2 \end{bmatrix} \tag{5.2}$$

The receiver may be calibrated to within the complex scalar a_1 by solving for A, B, and C. To measure A, B and C it is convenient to define the polarization ratio, $\rho = V/H$, and a similar ratio $\Gamma = V_2/V_1$. Equation (5.1) may be written in terms of Γ and ρ for the i^{th} measurement as

$$\Gamma_i = \frac{B + C\rho_i}{1 + A\rho_i} \tag{5.3}$$

By rotating a polarizing grid to three different positions, scattered waves having known polarization ratios, ρ_1, ρ_2 and ρ_3, will be generated. A, B, and C are then found by measuring $\Gamma_1, \Gamma_2, \Gamma_3$ associated with ρ_1, ρ_2, ρ_3. One may measure A, B and C by selecting ρ_1, ρ_2 and $\rho_3 = 0$, -1, and ∞. A, B, and C are then given by

$$\begin{aligned} A &= \frac{\Gamma_1 - \Gamma_2}{\Gamma_3 - \Gamma_2} \\ B &= \Gamma_1 \\ C &= \Gamma_1 - \Gamma_2(1 - A) = \Gamma_3 A \end{aligned} \tag{5.4}$$

The Stokes vectors of the four transmit waves may be precisely characterized by use of the calibrated receiver and an odd-bounce reflector, that preserves the polarization state of the reflected wave. This procedure involves measuring V_1 and V_2 for a given transmit polarization, solving for H and V using (5.2) then computing the transmit Stokes vector using (2.7). The radar may now be used to measure the relative Stokes matrix of any target using the procedure just described to find the received Stokes vectors, $\mathbf{r}_i$, then solving (2.12) for M. A

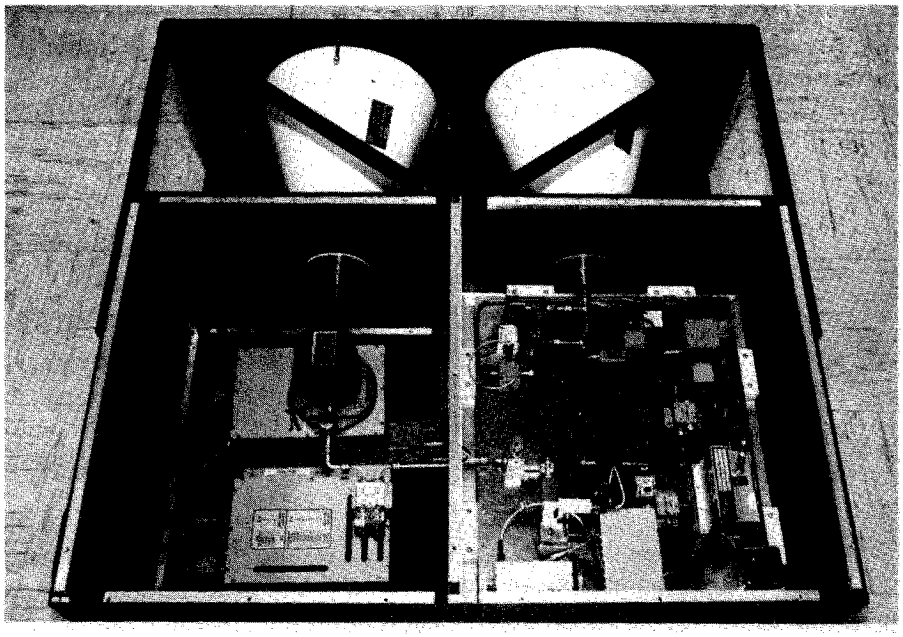

Figure 8.28 95 GHz polarimetric radar.

standard absolute calibration technique is used to find the absolute magnitude of M.

8.6 Examples of Millimeter-Wave Polarimeters

In this section, we present two pulsed millimeter-wavelength polarimeters that have been designed for experimental measurements of various geophysical targets such as trees, snow and hydrometeors. The first is a coherent 95 GHz radar capable of measuring the instantaneous scattering matrix in two pulses. The second radar described is an incoherent 225 GHz radar, capable of measuring the average Stokes matrix of a target by manually switching transmit polarizations.

a. Coherent, 95 GHz Polarimetric Radar

A system diagram for a coherent 95 GHz polarimetric radar designed and fabricated by the University of Massachusetts for terrestrial and atmospheric measurements is shown in Fig. 8.27. The system consists of a common PLO reference, which acts as both receiver local

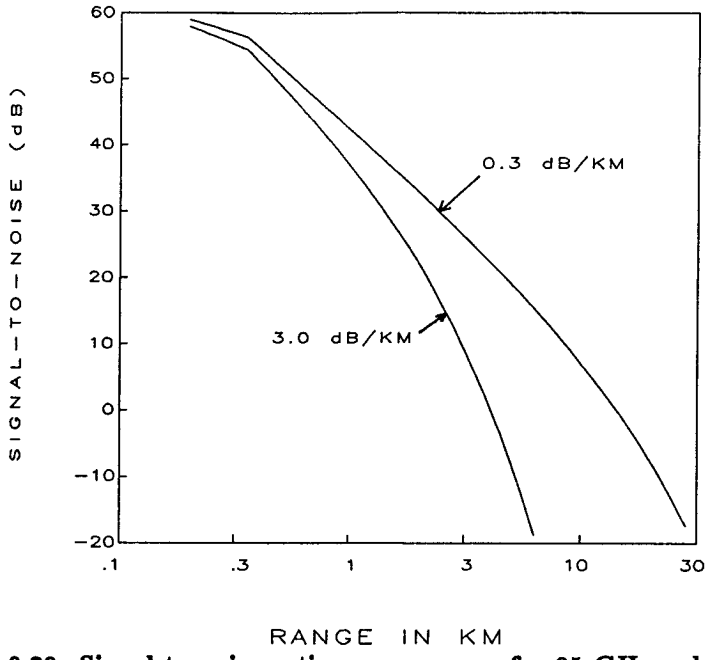

Figure 8.29 Signal-to-noise ratio versus range for 95 GHz polarimeter with atmospheric loss as a parameter.

oscillator and driver for the transmitter amplifier chain. The transmitter amplifier consists of a two-stage, solid-state amplifier followed by an Extended Interaction Amplifier (EIA), manufactured by Varian, Canada. Alternate transmission of vertically and horizontally polarized 95 GHz pulses is achieved with a waveguide ferrite switch. An orthomode transducer is used to separate the horizontally and vertically polarized components of the scattered signal, which is received by a 1.32 GHz using single-balanced mixers employing Schottky-barrier beam lead diodes. The received voltage is downconverted common polarization insensitive antenna. The signal is then amplified and downconverted again to 120 MHz where the signal is divided for separate amplitude and phase detection. A log amplifier/detector is employed in the amplitude channels, providing a dynamic range of 80 dB. The phase detector is preceded by a constant phase limiter, which maintains nearly constant phase over a dynamic range of 70 dB. The limiter maintains a constant input voltage to the I/Q detector, which has a limited dynamic range. System specifications are given in Table 8.2 and specifications for the EIA and other millimeter-wave components

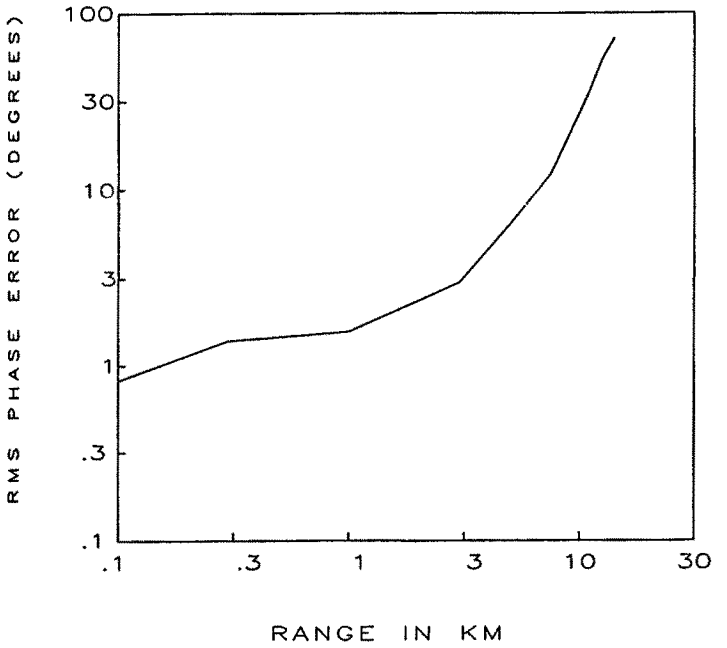

Figure 8.30 RMS phase noise versus range for UMass 95 GHz polarimeter.

used in this radar are given in Table 8.3. A photograph of the 95 GHz polarimeter is shown in Fig. 8.28.

The range capability of this instrument was analyzed using the radar range equation for surface targets [Nathanson, 1969] and a plot of SNR versus range for a surface having $\sigma_0 = -10$ dB is shown in Fig. 8.29 for various atmospheric conditions. To estimate the accuracy of phase measurements, the various terms in (4.11) were evaluated for this radar. These values are listed in Table 8.4. By computing the phase error due to thermal noise from the SNR values in Fig. 8.29 (using a nominal atmospheric loss of 1 dB $\cdot$ km^{-1}), the net RMS phase error versus range was computed and plotted in Fig. 8.30.

b. 225 GHz Polarimeter

The 225 GHz polarimeter consists of a multiple polarization transmitter, a dual polarization receiver, the Polarimetric Radar Control and Data Acquisition (PRACDA) subsystem, and a data logging computer. During polarimetric measurements, the transmitter's multiple-polarization lens antenna is sequentially switched between the four po-

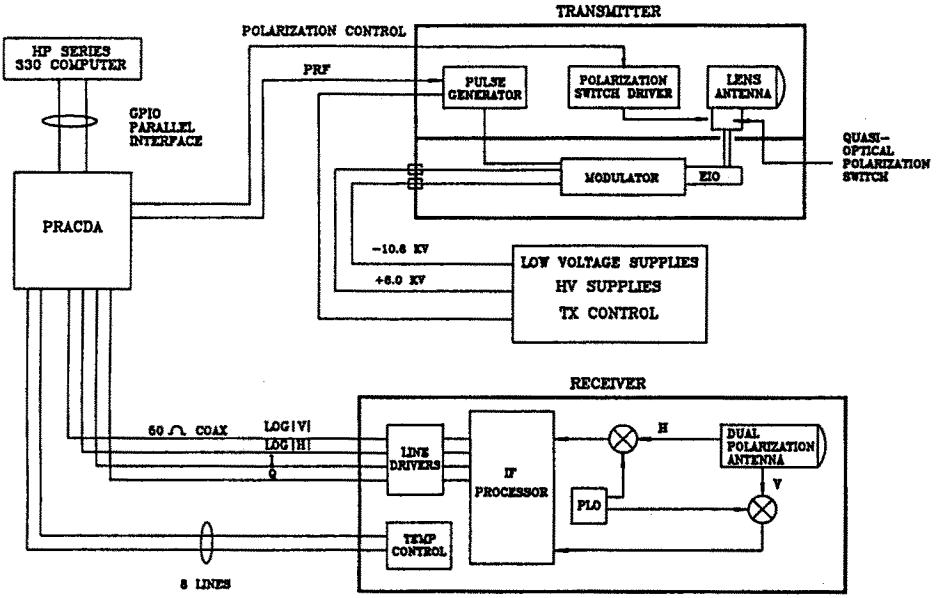

Figure 8.31 225 GHz polarimeter system block diagram.

larization states given in (2.9). The magnitude of the vertical and horizontal components of the scattered wave along with the phase difference between these components is measured using a dual-polarization receiver for each transmit state. This provides sufficient information to determine the received Stokes vector, **r**, using (2.7). The transmitter, receiver and data acquisition subsystems are described in detail below. A block diagram of the system is shown in Fig. 8.30. In addition, the electrical characteristics of the polarimeter system are summarized in Table 8.5. Table 8.6 gives specifications for various components.

b.1 Transmitter description

Much of the transmitter circuitry including the modulator, driver and pulse generator, were built at the Georgia Tech Research Institute [1982]. The transmitter employs an Extended Interaction Oscillator which produces a 60 W pulse of 50–600 nS duration. The transmitter antenna subsystem is shown schematically in Fig. 8.31. A scalar horn is used to illuminate a 6 inch diameter lens through two quarter-wave plates that can be independently rotated to control the polarization state. The lens material is TPX® (poly 4-methylpentene-1) which has

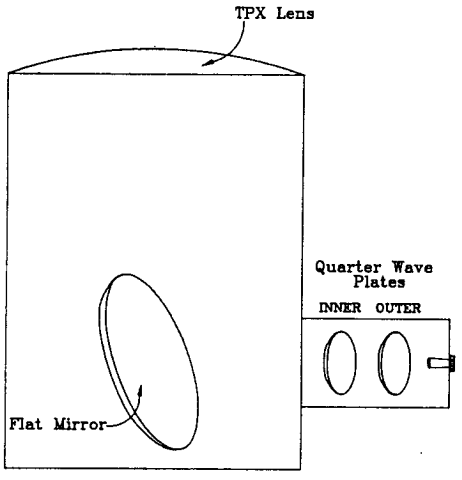

Polarization	Inner (Φ)	Outer
Horizontal	0°	0°
Vertical	45°	45°
45° Linear	22.5°	22.5°
Right Cir.	−45°	0°
Left Cir.	45°	0°

Figure 8.32 Multiple polarization lens antenna.

an index of refraction of $n = 1.458$. The lens has a focal length-to-diameter ratio of $f/d = 2$ and has a nominal beamwidth of .61°. By rotating the two quarter-wave plates through an angle ϕ, the linearly-polarized output wave is rotated by 2 ϕ with respect to the horizontal. To achieve right or left hand circular polarization the outer plate is held fixed while the inner plate is rotated ±45°. The quarter-wave plates are rotated by a chain drive system powered by stepper motors that are controlled by the data acquisition system in order to automate the measurement process. A photograph of the transmitter is shown in Fig. 8.33.

b.2 Receiver

Figure 8.34 is a block diagram of the receiver showing its major functional components. The antenna, mixers, local oscillator and phase-lock circuitry were provided as an integrated subsystem by Millitech Corporation. The dual polarization antenna uses a six inch diameter TPX® lens with $f/d = 1$. The vertically and horizontally polarized components (V and H) of the incoming field are separated by a linear array of 0.001 inch diameter wires that are spaced at 300 wires per inch.

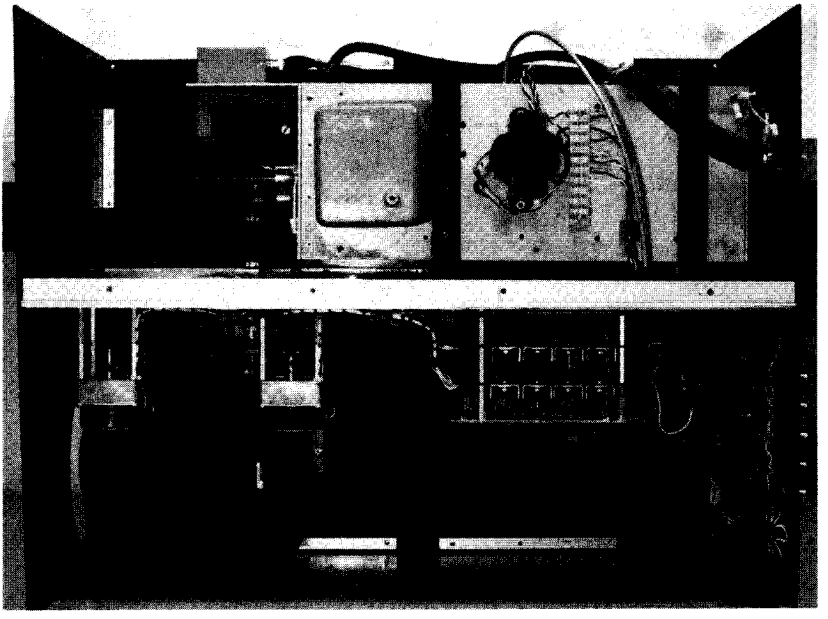

Figure 8.33 Top view of transmitter showing modulator and EIO (top).

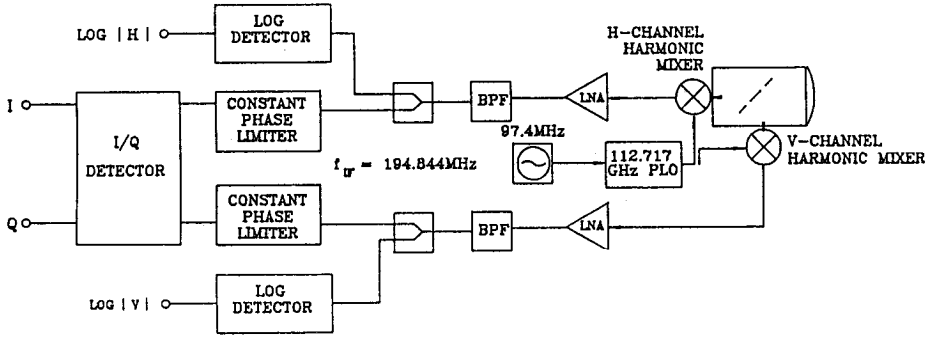

Figure 8.34 Receiver block diagram.

TRANSMITTER	
Center Frequency	94.92 GHz
Peak Output Power	1000 W
Pulse Width	50–1000 ns
PRF, Max.	80 KHz
RECEIVER	
SSB Noise Figure	10 dB
IF Bandwidth	Up to 40 MHz
Dynamic Range	70 dB
Outputs	$\log\|V\|, I_V, Q_V$ $\log\|H\|, I_H, Q_H$
Dynamic Range	75 dB
ANTENNA	
Receiver	Dual polarized lens, H and V channels, .7° beamwidth
Transmitter	Polarization insensitive lens, with polarization switch for various linear polarizations, .7° beamwidth

Table 8.2 Characteristics of UMass 95 GHz Polarimeter Radar

Scalar feed horns are attached directly to the input of the harmonic mixers to minimize losses. The second harmonic mixers are pumped with an LO of 112.717 GHz at a power level of approximately 10 mW. The LO consists of an InP Gunn oscillator, which is phase-locked to a 97.4 MHz crystal oscillator. If desired, the LO may be tuned from 112.4 to 112.9 GHz using a tunable low phase-noise reference resulting in approximately 1 GHz bandwidth centered at 225.63 GHz. An IF matching network having a passband of 50 to 500 MHz is provided at the output of the harmonic mixers. A short semirigid coaxial cable connects the matching network to a Low Noise Amplifier (LNA) with 46 dB gain and a noise figure of 1 dB. The receiver sensitivity was measured radiometrically using the Y-factor method from which the DSB noise figures of the H and V channels were found to be 11.8 and 11.2 dB, respectively.

The receiver IF consists of separate magnitude and phase detection channels. The magnitude of V and H are sampled independently by log detectors having a dynamic range of 70 dB. The relative phase between V and H is measured by an In-phase and Quadrature (I-Q)

Extended Interaction Amplifier	Manufacturer: Varian of Canada Part No. VKB 2461 Gain: 45 dB, min. Power output: 1 kW, min. Electronic Tuning Bandwidth: 350 MHz Mechanical Tuning Bandwidth: 1 GHz Maximum Duty Cycle: .01
Polarization Switch:	Manufacturer: Alpha Industries Part No. W145 Insertion Loss: .7 dB Cross Polarization Isolation: 20 dB Bandwidth: 3 GHz P_{ave}: 1.5 W P_{peak}: 500 W Switching Speed: 5 μs
Orthomode Transducer:	Manufacturer: Alpha Industries Part No. W881 Isolation: 30 dB Bandwidth: 3%
Single Balanced Mixers:	Manufacturer: Millitech Corporation Part No. MXP–10 Conversion Loss: 5.5 dB 1 dB Compression Point: +3dBm LO Drive: +10 dBm LO/RF Isolation: 20 dB LO/IF Isolation: 30 dB
Antenna	Manufacturer: Alpha Industries Part No.: 858012W Lens Material: Rexolite®

Table 8.3 95 GHz Hardware Specifications

Source of Errors	RMS Phase Error
(a) Phase Noise of 94 GHz PLO	$\sigma_{PLO} = 2.2°$
(b) Thermal Noise of Receiver	See Figure 21
(c) Quantization Error	$\sigma_{A/D} = .46°$
(d) Mechanical Vibrations (less than 2 g acceleration)	σ_M = less than .5°
(e) Temperature Variations (less than 10° C)	σ_T = less than .5°

Table 8.4

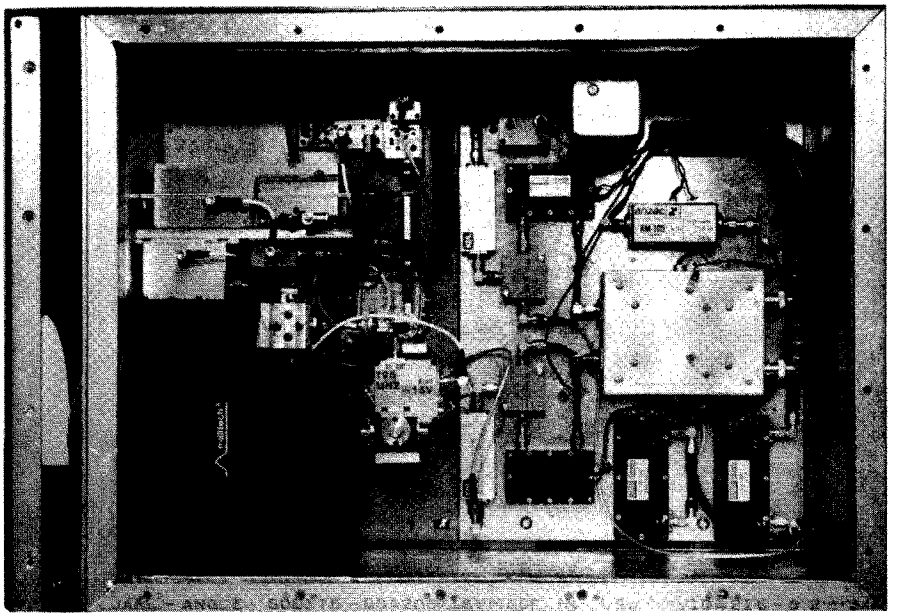

Figure 8.35 Top view of receiver showing mm-wave components (left) and IF (right).

detector, which is preceded by matched constant phase limiters that provide a constant 10 dBm output over more than 65 dB dynamic range. Measuring the magnitude of V and H and their relative phase completely specifies the polarization state of the sampled wave and determines the Stokes vectors of the scattered waves.

The entire receiver, including antenna, millimeter wave front-end and the IF section are temperature stabilized to minimize phase changes in the vertical and horizontal channels and stabilize the transfer characteristics of other receiver components. A controller mounted in the receiver box samples thermistor voltages from eight locations within the receiver and is used to control heaters and a fan. The computer periodically samples the thermistor voltages and keeps a record of the corresponding temperatures. A photograph of the receiver's millimeter-wave and IF sections is shown in Fig. 8.35.

b.3 Data acquisition system

The data acquisition subsystem consists of four 20 MHz, 8-bit A/D converters, a 150 bit status register that stores the various radar

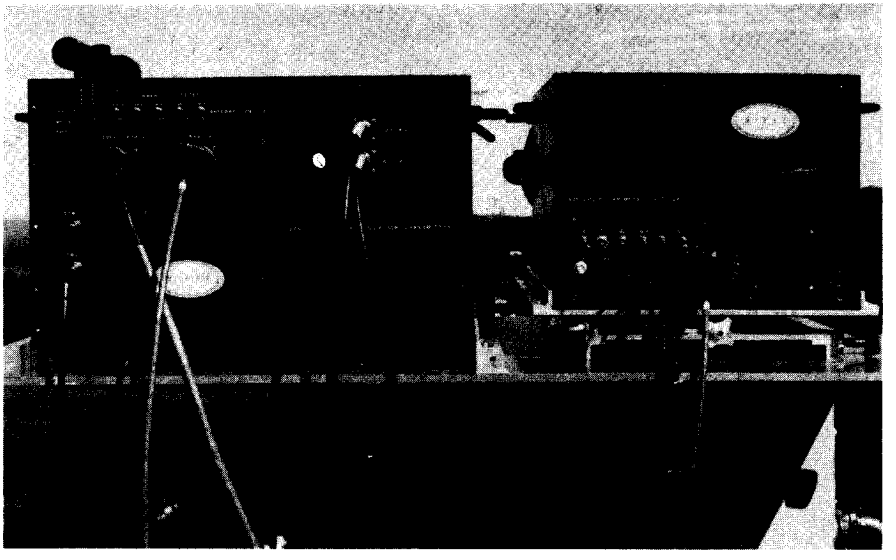

Figure 8.36 Transmitter (near) and receiver mounted on azimuth-over-elevation positioner.

states, and circuitry to interface with the data logging computer via a General Purpose Input/Output (GPIO) bus. The status registers are used to control the radar's PRF, number and position of the range gates, and the transmitter polarization. Data is acquired through four inputs that pass through a sample and hold circuit before being digitized. A First-in First-out (FIFO) buffer allows as many as 64 range gates to be sampled in rapid succession (100 nS minimum gate spacing). The data is then transferred asynchronously via the GPIO bus.

The transmitter and receiver are shown together in Fig. 8.36, mounted on an azimuth-over-elevation positioner used for field measurements from the roof of a 70 meter high building. The vertical channel response of a 3″ trihedral corner reflector (σ = 79.9 m^2) to a vertically polarized transmitted wave (i.e., the V–V response) at a range of 315 meters is shown in Fig. 8.37. The noise floor of −53 dBm is shown for comparison. From this measurement, we conclude that a 10 m^2 target will be visible above the noise floor (B = 50 MHz) at a range of 1.0 km.

Measurements of foliage, terrain, rain as well as various artificial

Transmitter	
Center Frequency	225.63 GHz
Output Power, Peak	60 W
Duty Cycle, Maximum	.005
PRF, Maximum	20 KHz
Pulse Width	50–500 ns
Receiver	
SSB Noise Figure	15 dB
F_{IF}	194.8 MHz
IF Bandwidth	Up to 50 MHz
Outputs	$\log\|V\|, \log\|H\|, I_{rel}, Q_{rel}$
Dynamic Range	70 dB
Antennas	
Receiver	Dual Polarization, H and V Channels, .61° Beamwidth
Transmitter	Multiple Polarization, Manually Switchable, .61° Beamwidth

Table 8.5 Specifications for 225 GHz Polarimetric Radar

Extended Interaction Oscillator	Manufacturer: Varian of Canada Model No. VKY–2429R Anode Bias: −10 kV Cathode "On" Bias: −19 kV Max. Beam Current: −8 mA, Ave.
Receiver Mixers	Manufacturer: Millitech Corporation Model No. MX5–05 F_{LO}: 112.72 GHz LO Drive Requirement: +6 dBm F_{IF}: 194.8 MHz Conversion Loss: 14 dB 1 dB Compression Point: −4 dBm
Antennas	Manufacturer: Millitech Corporation Lens Material: TPX®

Table 8.6 Hardware Specifications for 225 GHz Radar

targets were performed during the summer of 1989. Measurements of a vertically oriented dihedral corner reflector made at a range of 200 meters are shown in Fig. 8.38, as a function of the orientation angle, ϕ and ellipticity angle, τ, of the transmitter polarization. For the copolarized signature, the receiver antenna has the same polarization state

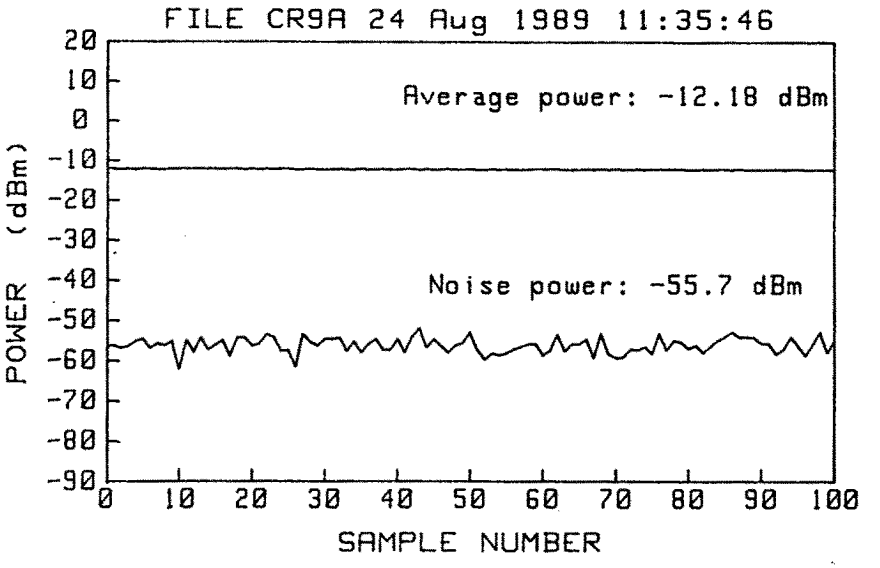

Figure 8.37 Return from 3-inch corner reflector at a range of 315 meters. Also shown is the thermal noise floor.

as the transmitter antenna, whereas the receiver and transmitter antenna polarizations are orthogonal in the cross-polarized signature. The minima of the co-polarized/cross-polarized signatures that are seen at $\phi = 45°$ and 135°, and $\tau = 0°$ are typical for this type of point target [Huynen, 1970]. The minima of the co-polarized signature also are at those orientation and ellipticity angles at which maxima values of the cross-polarized signature occur.

Measured co-polarized signatures for an Eastern Cottonwood (deciduous) tree and a White Pine (conifer) tree shown in Fig. 8.2 are shown again in Figs. 8.39(a) and 39(b). Measured data indicates that the level of unpolarized energy decreases with increasing leaf/needle size. The degree of depolarization in the White Pine's response is better illustrated in Figs. 39c and 39d where we plot a power weighted histogram of the receive polarization state as a function of ϕ and τ when the transmit polarization is vertical. The power-weighted standard deviation of the received polarization ellipse angles, ϕ and τ, for

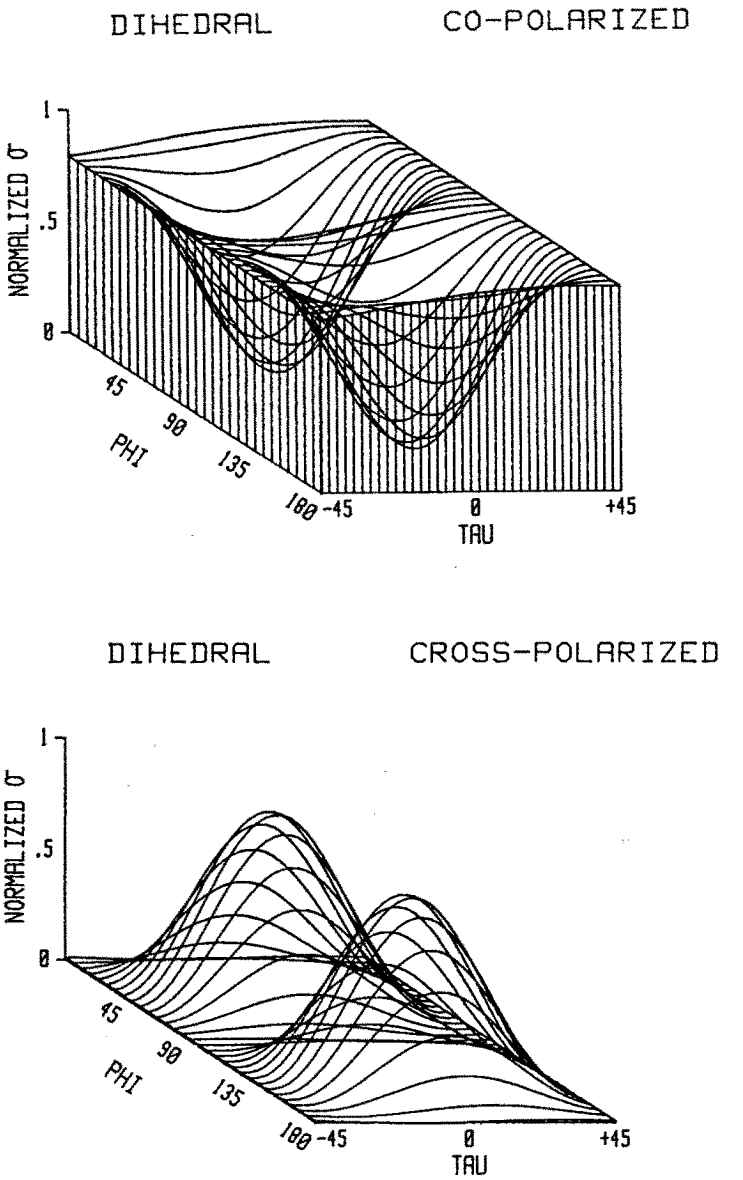

Figure 8.38 Co- and cross-polarized signature for a dihedral corner reflector.

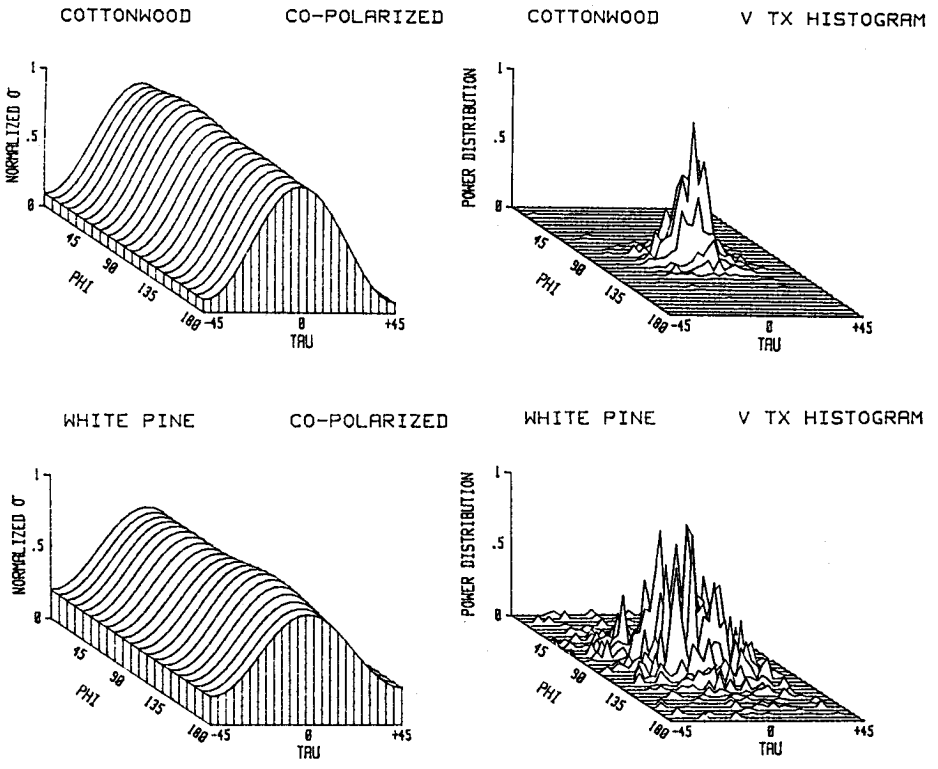

Figure 8.39 Co-polarized signatures for (a) Eastern Cottonwood and (b) White Pine. Scatter plot of received polarization state for (c) Eastern Cottonwood and (d) White Pine.

these measurements are: Cottonwood: $\sigma_\phi = 11.3°$ and $\sigma_t = 9.2°$; White Pine: $\sigma_\phi = 22.8°$ and $\sigma_t = 14.0°$.

References

[1] Chernov, L. A., *Wave Propagation in a Random Medium*, McGraw-Hill, New York, 1960.

[2] Clifford, S. F., J. W. Strohbehn, "The Theory of Microwave Line-

of-Sight Propagation Through a Turbulent Atmosphere," *IEEE Trans. Antennas and Propagation,* **AP-18**, 264–274, 1970.

[3] Cohn, M., J. E. Degenford, and B. A. Newman, "Harmonic Mixing with an Antiparallel Diode Pair," *IEEE Trans. Microwave Theory and Tech.,* **23**, 667–673, 1975.

[4] Covert, G., *Sub-millimeter Wave Generation using Conventional Means,* presented at the C. V. D. Sympo. on Millimeter Wave Generation, Sheffield University, England, 1961.

[5] Cox, D. C., H. W. Arnold, and A. J. Rustako, Jr., "Attenuation and Depolarization by Rain and Ice Along Inclined Paths Through the Atmosphere at Frequencies Above 10 GHz," *IEEE EASCON-79 Rec.,* **I**, 156–62, 1979.

[6] Cutler, L. S., and C. L. Searle, "Some Aspects of the Theory and Measurement of Frequency Fluctuations in Frequency Standards," *Proc. IEEE,* **54**, 136–154, 1966.

[7] Evans, D. L., T. G. Farr, J. J. van Zyl, and H. A. Zebber, "Radar Polarimetry: Analysis Tools and Applications," *IEEE Trans. Geosci. Remote Sens.,* **26**, 6, 774–789, 1988.

[8] Hogg, D. C., and T. S. Chu, "The Role of Rain in Satellite Communications," *Proc. IEEE,* **63**, 1308–1331, 1975.

[9] Hughes Microwave Products Division, *Hughes Millimeter-wave Products for 1987–1988,* Hughes Aircraft Company, Torrance, CA, 1987.

[10] Huynen, J. R., "Measurement of the Target Scattering Matrix," *Proc. IEEE,* **53**, 936–946, 1965.

[11] Huynen, J. R., *Phenomenological Theory of Radar Targets,* Ph.D. Dissertation, Drukkerij Bronder-Offset N.V., Rotterdam, 1970.

[12] Lhermitte, R. M., "Cloud and Precipitation Remote Sensing at 94 GHz," *IEEE Trans. Geosci. Remote Sens.,* **26**, 3, 207–216, 1988.

[13] Liebe, H. J., "An Updated Model for MM-Wave Propagation in Moist Air," *Radio Science,* **20**, 1069–1089, 1985.

[14] McMillan, R. W., J. C. Wiltse, and D. E. Snider, "Atmospheric Turbulence Effects on Millimeter Wave Propagation," *IEEE EASCON-79 Rec.,* **1**, 42–47, 1979.

[15] Meredith, R., and F. L. Warner, "Superheterodyne Radiometers

for Use at 70 Gc and 140 Gc," *IEEE Trans. Microwave Theory and Tech.*, **11**, 397–411, 1963.

[16] Mie, G., "Beitrage zur Optik truber Medien, Speziell Kolloidaler Metalasungen," *Ann. Physik*, **25**, 377, 1908.

[17] Millitech, *Millimeter and Submillimeter Components, Instruments, Subsystems*, Millitech Corporation, South Deerfield, MA, 1986.

[18] Morrison, J. A., and T. S. Chu, "Perturbation Calculations of Rain-Induced Differential Attenuation and Differential Phase Shift at Microwave Frequencies," *Bell Syst. Tech. J.*, **52**, 1907–1913, 1973.

[19] Nathanson, F. E., *Radar Design Principles*, McGraw-Hill, New York, 63–67, 1969.

[20] Oguchi, T., "Rain Depolarization Studies at Centimeter and Millimeter Wavelengths: Theory and Measurement," *J. Radio Research Labs.*, **22**, 165–211, 1975.

[21] Pan, S. K., et. al., "An SIS Mixer for 85-116 GHz using Inductively Shunted Edge-Junctions," *IEEE MTT-S Digest*, **I**, 465–468, 1988.

[22] Predmore, C. R., N. R. Erickson, G. R. Huguenin, and P. F. Goldsmith, "A Continuous Comparison Radiometer at 97 GHz," *IEEE Trans. on Micro. Theory and Tech.*, **33**, 44–51, 1985.

[23] Ruf, C., NASA, Jet Propulsion Lab., private communication.

[24] Saad, T. S., ed., *Microwave Engineers' Handbook Volume I*, Artech House, Inc., Dedham, MA, p. 36, 1971.

[25] Tatarski, V. I., *Wave Propagation in a Turbulent Medium*, McGraw-Hill, New York, 1961.

[26] Ulaby, F. T., R. K. Moore, and A. K. Fung, *Microwave Remote Sensing, Active and Passive, Volume I*, Addison-Wesley, 290–298, 1981.

[27] Van Vleck, J. H., "The Absorption of Microwaves by Uncondensed Water Vapor," *Phys. Rev.*, **71**, 425–433, 1947.

[28] van Zyl, J. J., *On the Importance of Polarization in Radar Scattering Problems*, Ph.D. Dissertation, California Institute of Technology, Pasadena, CA, Report 120, 1985.

[29] Viterbi, A. J., *Principles of Coherent Communications,* McGraw-Hill, New York, p. 94, 1966.

[30] Waters, J. W., "Absorption and Emission of Microwave Radiation by Atmospheric Gases," in *Methods of Experimental Physics,* M. L. Meeks, ed., **12**, Part B. Radio Astronomy, Academic Press, Section 2.3, 1976.

[31] Weinreb, S., M. W. Pospieszalski, and R. Norrod, "Cryogenic, HEMT Low-Noise Receivers for 1.3 to 43 GHz Range," *IEEE MTT-S Digest,* **2**, 945–948, 1988.